Study on the electrical and dielectric behaviour of Zn-substituted cobalt ferrialuminates

2006 J. Phys.: Condens. Matter 18 8063

(http://iopscience.iop.org/0953-8984/18/34/017)

INSTITUTE OF PHYSICS PUBLISHING JOURNAL OF PHYSICS: CONDENSED MATTER

J. Phys.: Condens. Matter **18** (2006) 8063–8092 doi:10.1088/0953-8984/18/34/017

Study on the electrical and dielectric behaviour of Zn-substituted cobalt ferrialuminates

N H Vasoya[1], V K Lakhani[1], P U Sharma[1], K B Modi[1], Ravi Kumar[2] and H H Joshi[1]

[1] Department of Physics, Saurashtra University, Rajkot-360 005, India
[2] IUAC, Aruna Asaf Ali Marg, New Delhi-110 067, India

E-mail: kunalbmodi2003@yahoo.com

Received 18 May 2006, in final form 3 July 2006
Published 11 August 2006
Online at stacks.iop.org/JPhysCM/18/8063

Abstract

The structural, electrical and dielectric properties of the spinel ferrite system $Zn_xCo_{1-x}FeAlO_4$ ($x = 0.2$–0.5) have been studied by means of various experimental techniques. Polycrystalline samples of this series have been prepared by the double sintering ceramic method. The structural parameters such as the lattice constant, x-ray density, pore fraction, cation distribution, interionic distances and polaron radius have been determined for better understanding of the electrical and dielectric behaviour. The compositional and thermal variations of the electrical properties have been studied by means of dc resistivity, thermoelectric power, I–V and C–V measurements. The electrical parameters such as the activation energy, Fermi energy, charge carrier concentration and mobility have been determined and a probable conduction mechanism in the system has been suggested. It is found that the ferrites are electronic conductors, and various results confirm the formation of small polarons. Current controlled negative resistance (CCNR)-type switching is observed in samples with $x = 0.3$–0.5. The dielectric behaviour of the system has been studied by measuring the dielectric constant, complex dielectric constant and conductivity in the frequency range 100 Hz–1 MHz at selected temperatures. The compositions exhibit normal dielectric behaviour, attributed to Maxwell–Wagner type interfacial polarization. Broadband dielectric spectroscopy in the form of an electric modulus has been applied to investigate the electrical spectroscopy in a wide temperature range. The results clearly indicate the presence of the non-Debye type of dielectric relaxation in these materials.

(Some figures in this article are in colour only in the electronic version)

1. Introduction

The field of ferrites is well cultivated, but due to their various potential applications and the interesting physics involved in them, even after more than half a century, scientists, researchers, technologist and engineers are still interested in various types of ferrite materials, substituted with different cations, prepared by different techniques, and their various properties as a function of composition, temperature, frequency, etc, in bulk, thin film and nanoparticle form.

The studies of electric and dielectric behaviour are equally important as those of the magnetic properties, from both the applied and fundamental research points of view. The electric properties such as dc resistivity, thermoelectric power and I–V/C–V characteristics provide vital information regarding the activation energy, Fermi energy, type of charge carriers responsible for conduction mechanism, carrier concentration, its mobility and related aspects.

Dielectric spectroscopy in a broad frequency range is widely used to study the electric and dielectric behaviour of various ceramics. One can obtain important information on the relaxation process occurring in the system from the dielectric frequency response curve at different temperatures. The dielectric properties of materials can be expressed in various ways, using different representations. Experimental data are usually reported in terms of both the temperature and frequency dependence of either the conductivity ($\sigma^* = \sigma' + \mathrm{i}\sigma''$), complex impedance ($Z^* = Z' - Z''$), the dielectric permittivity ($\varepsilon^* = \varepsilon' - \mathrm{i}\varepsilon'$) or the dielectric modulus ($M^* = M' + \mathrm{i}M''$) [1–3]. Although these alternative representations are equally valid, they may provide new insight into the dielectric and electrical properties of materials. A comparison of the complex dielectric permittivity (ε^*) and M^* representation allows us to distinguish the local dielectric relaxation (e.g. dipole reorientation) from long range electrical conductivity. It is possible to ascribe a given process to a specific mechanism based on values of the activation energy and the characteristic relaxation time.

In the domain of frequency, the dielectric response of a system subjected to an external oscillating electric field is fully characterized by the complex permittivity, $\varepsilon^*(\omega)$, where the real and imaginary components are the storage and loss, respectively, of the energy during each cycle of the electric field. Therefore, experimental data presented in terms of frequency dependent permittivity values is common practice. However, in the case of a semiconducting materials like spinel ferrite and garnets, analysis of relaxation processes in $\varepsilon^*(\omega)$ presentation is difficult due to the significant dc conductivity (conductivity at 0 Hz) contribution that obscures any relaxation process [4].

The physical properties of polycrystalline magnetic ceramics like ferrites are influenced by the shape, size and orientation of grains boundaries, voids, inhomogeneities, surface layers and contacts. Information about the associated physical parameters of the microstructural components is important since the property of the materials is determined by those components. Impedance spectroscopy is an important tool with which to investigate the electrical properties of partially blocking grain boundaries in electro-ceramic materials. The complex-plane impedance (Cole–Cole plots) representation is employed in separating various microstructural and external components. This is possible as the processes that are associated with the individual components are usually characterized by different time constants, so they respond at different frequency ranges.

The present work aims to carry out multifold studies in a comprehensive manner.

(i) Thermal variation of electrical properties of the $Zn_xCo_{1-x}FeAlO_4$ ($x = 0.2$, 0.3, 0.4 and 0.5) spinel ferrite system by means of dc resistivity, thermoelectric power, I–V and C–V characteristics measurements.
(ii) Compositional, temperature and frequency dependent dielectric behaviour in the frequency range 100 Hz–1 MHz for selected temperatures, and its presentation in the form of the dielectric modulus.

(iii) Study of the probable conduction mechanism, the phenomenon responsible for switching behaviour, electric relaxation properties, etc.

2. Experimental details

Four samples of the $Zn_xCo_{1-x}FeAlO_4$ spinel ferrite system were prepared by the usual double sintering ceramic method for $x = 0.2$, 0.3, 0.4 and 0.5. The starting materials were analytical reagent grade oxides, ZnO, CoO, Fe_2O_3 and Al_2O_3. These oxides were mixed in the proper proportions and pre-sintered at 1000 °C for 24 h. In the final sintering process the material was held at 1100 °C for 12 h and slowly cooled to room temperature at the rate of 2 °C min^{-1}. The x-ray diffractograms were obtained using Cu Kα radiation on a Philips x-ray diffractometer (model PW1710). The diffraction patterns show the sharp lines corresponding to a single-phase spinel structure for all the samples.

The samples for electric and dielectric measurements were in the form of discs 10 mm in diameter and 3 mm thick. Both the faces of each sample were polished by rubbing with zero grade emery paper; the samples were then washed in dilute HCL and acetone. Finally, graphite was rubbed on both flat faces of the samples on which aluminium foil was also attached for good electrical contacts. The resistance of a pellet was measured by the two terminal pressure contact method using a BPL megohm meter. Thermal variation of resistance was obtained by placing a sample holder containing a pellet in a horizontal electric furnace: the temperature was measured by a chromel–alumel thermocouple. The resistance of the pellet was measured during the decrease of temperature at steps of 20 °C.

A thermoelectric power study was carried out over the temperature range 300–550 K by the differential method. The temperature gradient was measured by two chromel–alumel thermocouples that were kept very close to the sample while the thermo-emf was measured with the help of a digital microvoltmeter with an accuracy of $\pm 3\%$. In order to achieve good thermal stability, the values of the thermo-emf were recorded during cooling. The sample was maintained at a given temperature for about 5–10 min. Current versus voltage measurements were performed in the voltage range 0–500 V using an Aplab high voltage dc regulated power supply (model 7332). The measurements were carried out for selected temperatures in the range 300–800 K. The ac electrical measurements were carried out using an Agilent (model 4284A) precision LCR meter in the frequency range 100 Hz–1 MHz at different temperatures ranging from 300 to 700 K. The value of the regression coefficient (χ^2), which indicates goodness of data fitting, was found to be near to unity for all the fittings carried out in the paper.

3. Results and discussion

3.1. Structural properties

The room temperature (300 K) x-ray diffraction pattern of each composition (figure 1) corresponded to well defined crystalline fcc phase, and confirmed the spinel structure. No reflections other than those belonging to a spinel structure were observed in the patterns. The positions of all the Bragg's peaks were used to obtain the interplanar spacing and these values were used to index the peaks using the DEBYE program. The compositional stoichiometry of the samples was ascertained by EDAX.

The concentration dependence of the lattice constant a with an accuracy of ± 0.002 Å determined from XRD data for $x = 0.2$–0.5 is given in table 1. The lattice constant gradually increases with increasing x, obeying Vegard's law [5]. Usually, in a solid solution of spinels within the miscibility range, a linear change in the lattice constant with the concentration of

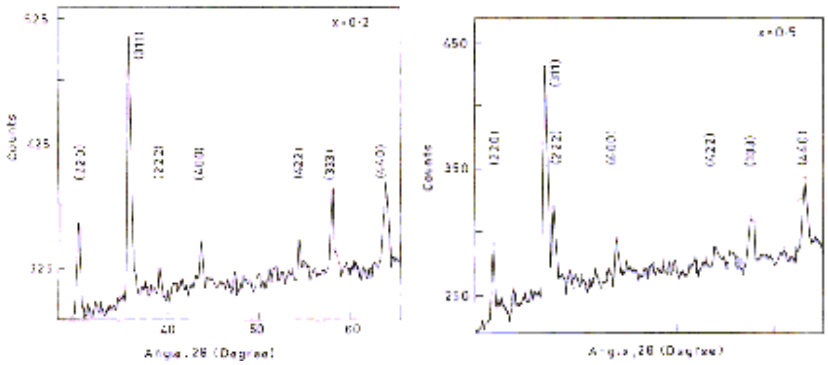

Figure 1. X-ray diffraction patterns for $x = 0.2$ and 0.5 compositions at 300 K.

Table 1. Lattice constant (a), unit cell volume (V_a), x-ray density (d_x), bulk density (d), pore fraction (f), ionic radius ($\bar{r}$), and anion parameter (u) for the Zn–Co–Fe–Al–O system.

Content (x)	a (Å) ±0.002 Å	V_a (Å)^3	d_x (kg m^{-3}) × 10^3	d (kg m^{-3}) × 10^3	f	r_A (Å)	r_B (Å)	u (Å)
0.2	8.3230	576.55	4.772	4.199	0.120	0.6710	0.6026	0.2657
0.3	8.3275	577.49	4.779	4.344	0.091	0.6769	0.5996	0.2661
0.4	8.3300	578.01	4.790	4.311	0.100	0.6828	0.5976	0.2664
0.5	8.3360	579.26	4.794	4.410	0.080	0.6900	0.5950	0.2669

the components is observed [5]. The slow linear increase in the lattice constant is due to the replacement of Co^{2+} (0.72 Å) ions by slightly larger Zn^{2+} ions with an ionic radius of 0.74 Å in the system $Zn_xCo_{1-x}FeAlO_4$. The x-ray density ($d_x = ZM_w/Na^3$; Z is the number of molecules per unit cell ($Z = 8$) of the spinel lattice, M_W is the molecular weight of the ferrite sample, N is Avogadro's number and a the lattice constant) and pore fraction ($f = 1 - d/d_x$; d = bulk density) values thus calculated for different Zn concentration (x) are summarized in table 1.

In order to determine the cation distribution, x-ray intensity calculations were made using the formula suggested by Buerger [6]:

$$I_{hkl} = |F_{hkl}|^2 P L_p$$

where I_{hkl} is the relative integrated intensity, F_{hkl} is the structure factor, P is the multiplicity factor and L_p is the Lorentz polarization factor $(1 + \cos^2\theta/\sin^2\theta\cos\theta)$.

According to Ohnishi and Teranishi [7], the intensity ratios of planes $I(220)/I(400)$, $I(220)/I(422)$ and $I(400)/I(422)$ are considered to be sensitive to the cation distribution parameter (x). The ionic configuration based on site preference energy values proposed by Miller [8] for individual cations in $Zn_xCo_{1-x}FeAlO_4$ suggest that Zn^{2+} and Al^{3+} have strong A-site and B-site preference respectively, while Co^{2+} and Fe^{3+} ions occupy the A- and B-sites. There is a good contrast in the atomic scattering factors of Fe^{3+} and the other cations present in the system. This makes the determination of cation distribution quite reliable. Moreover, any alternation in the distribution of cations causes a significant change in the theoretical values of x-ray diffraction intensity ratios. Therefore, in the process of arriving at the final cation distribution, the site occupancy of all the cations was varied for many combinations and those that agree with the experimental intensity ratios are shown in table 2. The final cation

Table 2. Comparison of x-ray intensity ratios for estimating cation distribution.

			$I(220)/I(400)$		$I(220)/I(440)$		$I(400)/I(422)$	
x	A-site	B-site	Cal.	Obs.	Cal.	Obs.	Cal.	Obs.
0.2	$Zn^{2+}_{0.20}Fe^{3+}_{0.40}Co^{2+}_{0.30}Al^{3+}_{0.10}$	$Fe^{3+}_{0.60}Co^{2+}_{0.51}Al^{3+}_{0.89}$	2.328	2.409	1.432	1.582	1.223	1.222
0.3	$Zn^{2+}_{0.30}Fe^{3+}_{0.43}Co^{2+}_{0.20}Al^{3+}_{0.07}$	$Fe^{3+}_{0.57}Co^{2+}_{0.50}Al^{3+}_{0.93}$	1.863	1.971	1.118	1.136	1.549	1.601
0.4	$Zn^{2+}_{0.40}Fe^{3+}_{0.46}Co^{2+}_{0.10}Al^{3+}_{0.04}$	$Fe^{3+}_{0.54}Co^{2+}_{0.50}Al^{3+}_{0.96}$	1.830	1.860	1.498	1.542	1.630	1.720
0.5	$Zn^{2+}_{0.50}Fe^{3+}_{0.50}$	$Fe^{3+}_{0.50}Co^{2+}_{0.50}Al^{3+}_{1.0}$	1.439	1.529	0.721	0.897	1.650	1.810

distributions were deduced by simultaneously considering the Bragg plane ratios and the fitting of the magnetization data at 80 K.

It is worthwhile noting that for unsubstituted ferrite ($CoFeAlO_4$; $x = 0.0$) around 37% of Fe^{3+}, 48% Co^{2+} and 16% of Al^{3+} occupy the A-site [9]. On substituting Zn^{2+}, having strong A-site preference, it replaces Co^{2+} from the system as well as from the A-site and transfers Al^{3+} ions from A-site to B-site. The study has revealed the B-site preference of Co^{2+}, Fe^{3+} and Al^{3+} as follows: $Al^{3+} \geqslant Co^{2+} > Fe^{3+}$.

Besides using experimentally found values of the lattice constant and oxygen position parameter (u) [10], it is possible to calculate the value of the mean ionic radius per molecule of the tetrahedral and octahedral sites, r_A and r_B respectively, using the cation distribution for each composition, from the relation [11]

$$r_A = [C_{AZn}r(Zn^{2+}) + C_{ACo}r(Co^{2+}) + C_{AFe}r(Fe^{3+})]$$
$$r_B = (1/2)[C_{BCo}r(Co^{2+}) + C_{BAl}r(Al^{3+}) + C_{BFe}r(Fe^{3+})]$$

where $r(Zn^{2+})$, $r(Fe^{3+})$, $r(Al^{3+})$, $r(Co^{2+})$ are the ionic radii of Zn^{2+}, Fe^{3+}, Al^{3+} and Co^{2+} ions respectively, while C_{AZn}, C_{AFe}, C_{ACo} are the concentration of Zn^{2+}, Fe^{3+} and Co^{2+} ions on A-sites and C_{BFe}, C_{BAl} and C_{BCo} are the concentrations of Fe^{3+}, Al^{3+} and Co^{2+} ions on B-sites.

Using these formulae, the values of mean tetrahedral and octahedral ionic radii for each composition have been calculated, and they are listed in table 1. It can be seen that the mean tetrahedral ionic radius increases continuously with increasing x. It is observed that ionic radius of the octahedral site decreases with increasing x. As such, it can be concluded that in the present system tetrahedral site substitution plays a dominant role in influencing the value of the lattice constant.

The oxygen positional parameter or anion parameter (u) for each composition was calculated using the formula [12]

$$u^{3m} = \frac{\frac{1}{4}R^2 - \frac{2}{3} + \left[\frac{11}{48}R^2 - \frac{1}{18}\right]^{\frac{1}{2}}}{2R^2 - 2}$$

where R = B–O/A–O. The bond lengths B–O and A–O are average bond lengths, based on the cation distribution listed in table 2; B–O $= \langle r_B + r(O^{-2})\rangle$ and A–O $= \langle r_A + r(O^{-2})\rangle$, where $r(O^{-2})$ is the radius of the oxygen ion.

The configurations of ion pairs in spinel ferrites with favourable distance and angle for effective magnetic interactions are shown in figure 2. The bond lengths between the cations (b, c, d, e and f) (M_e–M_e) and between the cation and anion (p, q, r and s) (M_e–O) were calculated using the experimental values of lattice constant and oxygen positional parameter

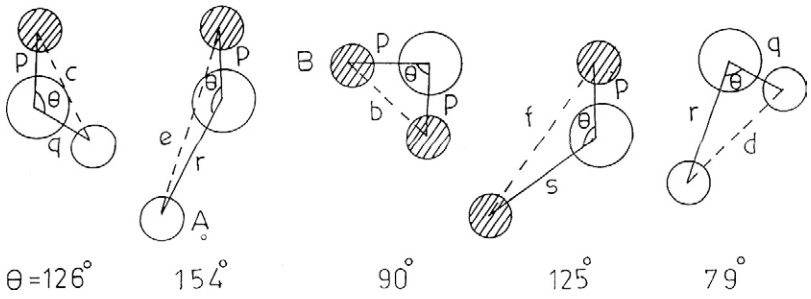

Figure 2. Configurations of the ion pairs in spinel ferrites with favourable distances and angles for effective magnetic interactions.

(u) by the relations [13, 14]

M_e–O	M_e–M_e
$p = a(1/2 - \bar{u})$	$b = (a/4)2^{1/2}$
$q = a(\bar{u} - 1/8)3^{1/2}$	$c = (a/8)11^{1/2}$
$r = a(\bar{u} - 1/8)11^{1/2}$	$d = (a/4)3^{1/2}$
$s = a/3(\bar{u} + 1/2)3^{1/2}$	$e = (3a/8)3^{1/2}$
	$f = (a/4)6^{1/2}$

It is seen that the bond lengths M_e–O and M_e–M_e increase with increasing concentration x. The increase in M_e–O and M_e–M_e distances should result in the weakening of the strength of interatomic bonding and as a result one can expect a reduction in the Néel temperature on Zn substitution.

Theoretical determination of Néel temperature. The Néel temperatures have also been calculated theoretically for $x = 0.2$–0.5 compositions by applying molecular field theory and using cation distribution (table 2). The Néel temperature depends upon the active magnetic linkages per magnetic ion per formula unit [15]. The statistical model proposed by Gilleo and Geller [15] has been found to hold reasonably well for non-magnetic substitution in spinel ferrites like $MgFe_2O_4$, $ZnFe_2O_4$, in which the magnetic ion (Fe^{3+}) concentration remains unaltered. When a magnetic/non-magnetic substitution is made for Fe^{3+}, it becomes too complex to estimate the Néel temperature. We have used a modified molecular field theory as suggested by Baldha *et al* [16] for Zn^{2+}-substituted cobalt ferrite. This involves A–A, A–B, and B–B interactions. $T_N(x)$ for a spinel ferrite doped with non-magnetic ion (Zn^{2+}) with concentration x for the magnetic $Co^{2+}(3\mu_B)$ ion can be expressed in terms of the Néel temperature of unsubstituted spinel ferrite ($T_N(x = 0.0)$) i.e. $CoFeAlO_4$ ($T_N = 580$ K [9]) by the equation:

$$T_N(X) = \frac{M(x = 0.0)T_N(x = 0.0)n(x)}{n(x = 0.0)M(x)}. \tag{1}$$

Here, $M(x)$ is the relative weighted total magnetic ions per formula unit, calculated by considering the weighting of the magnetic ion concentration for the substituted ferrite to that of the unsubstituted one. Thus, $M(x)$ for $Zn_xCo_{1-x}FeAlO_4$ can be expressed as

$$M(x) = 5 + \frac{3(1 - x)}{3} = 6 - x. \tag{2}$$

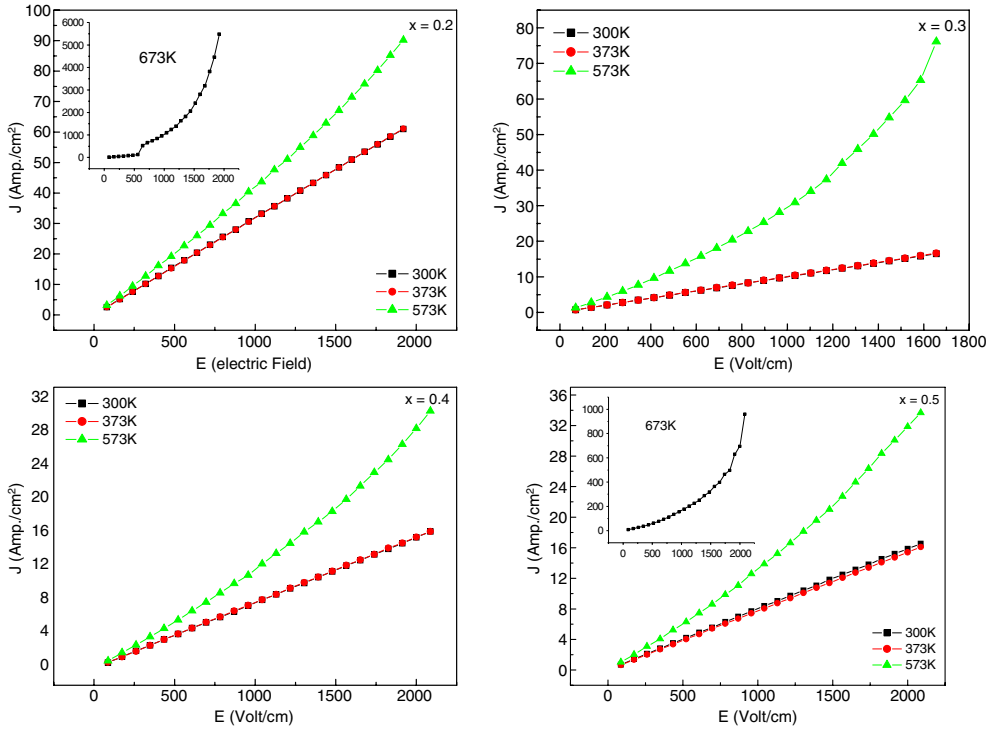

Figure 3. Variation of electric current density (J) with applied electric field (E) for $x = 0.2$, 0.3, 0.4 and 0.5 compositions.

$n(x)$ is the number of interactions per magnetic ion per formula unit, expressed as

$$n(x) = \left[\sum_{i,j=1}^{2} A_i B_j \mu_i \mu_j\right] \tag{3}$$

where A_i and B_j are the fraction of magnetic ions on the A- and B-sites, respectively, while μ_I and μ_j are the magnetic moments of the cation involved. Here $i, j = 1$ stands for magnetic ions other than Fe^{3+}, i.e. Co^{2+}, and $i, j = 2$ stands for iron.

The Néel temperature estimated using the above equations (1)–(3) are in good agreement with the Néel temperatures obtained from ac susceptibility [17] and dc resistivity measurements (table 4). This also indirectly supports the validity of cation distribution within that range. The values $T_N(x)$ thus determined for all the compositions are listed in table 4.

3.2. Electrical properties

For precise electrical measurements such as resistivity and thermoelectric power, ohmic contact is the first stringent requirement [18]. To ascertain the ohmic contact between pellet and electrode interface the current through each pellet was measured as a function of applied dc voltage at constant temperature and the results were plotted as J (current density) against E (applied electric field). Typical plots for compositions $x = 0.2, 0.3, 0.4$ and 0.5 are shown in figure 3. Reversal of the electric field does not have any effect on these measurements. It is seen that the J–E plots are linear in the applied electric field range from 1 to 600 V cm^{-1}, indicating the presence of ohmic contacts at the pellet–electrode interface in the temperature range of the

measurements. Of course, for $x = 0.2$–0.5 a deviation from linearity has been observed for $E > 600$ V cm^{-1} at high temperature ($T \geqslant 573$ K), indicating non-ohmic contact. Therefore, the electric field strengths that guarantee ohmic contact were used.

The compositional dependence of resistivity (ρ_{dc}) at 413 K is represented in table 4. It was observed from table 1 that the highest observed value of bulk density (d) remains less than the x-ray density (d_x) of the material. This indicates that even highly pressed and sintered pellets contain pores. Therefore, a correction for pore fraction has to be applied to obtain the crystalline value of electrical resistivity. This has been done using the relation [19]

$$\rho = \rho_p[1 + f(1 + f^{2/3})^{-1}]^{-1} \tag{4}$$

where ρ is the corrected value, ρ_p is the measured value of dc resistivity and f is the pore fraction (table 1). Equation (4) seems to hold good for $f < 0.4$.

We have correlated the jump length (L) of the charge carriers between Fe^{3+} and Fe^{2+} ions (for n-type conduction; $x = 0.2$, 0.3 and 0.4) and Fe^{4+} and Fe^{3+} (for p-type conduction; $x = 0.5$) on the octahedral site to the electrical resistivity. The jump length (L) is determined from the relation [20]

$$L = a\sqrt{2}/4$$

where a is the lattice constant (table 1). The values of jump length L for various values of Zn content (x) are summarized in table 4. This shows that L increases with increasing content x. The observed increase in L with x suggests that charge carriers require more energy to jump from one cationic site to other, which causes an increase in resistivity with increasing x. The present result on the variation of dc resistivity with x shows that ρ_{dc} decreases with increasing x (table 4). This is rather unexpected, because the replacement of magnetic Co^{2+} ions by non-magnetic Zn^{2+} ions, which do not participate in the conduction process, reduces conduction through the octahedral sites; as a result an increase in resistivity value with increasing Zn content may be expected. This discrepancy can be explained on the basis that the Zn ions have been evaporated from the surface layer at high sintering temperature and, as a result, ferrous ions (Fe^{2+}) have been formed and they occupy the B-sites. During heating, some of Fe^{2+} ions have been transformed to Fe^{3+} ions and this generates electrons, which participate in the conduction mechanism [21]. The simultaneous presence of Fe^{2+} and Fe^{3+} ions on equivalent lattice sites (B-sites) may cause the low surface resistivity. The large number of electrons that are generated during the transformation process will raise the conduction state of the system.

The thermoelectric power or Seebeck coefficient (α) does not show any pressure dependence within the accuracy of our measurement and does not warrant correction for pore fraction. Even after correcting for pore fraction, it is essential to see how significant the grain boundary effects are. To see this, ρ_{ac} was measured as a function of applied signal frequency at constant temperatures for all the ferrites, and typical plots for $x = 0.2$ and 0.4 compositions are shown in figure 4. It has been observed that the variation of ρ_{ac} is sensitively dependent on the frequency and temperature. This indicates that grain boundary effects are not sufficiently minimized for highly pressed pellets even at higher temperatures.

The first step in the understanding of electrical transport in any solid is to know whether the conductivity is ionic, electronic or mixed (partially ionic and electronic). There are several ways of determining this [22]. It is known that in the case of pure ionic conduction, ρ_{dc} increases with time and tends to become infinite after a sufficiently long time; whereas for a pure electronic conductor it is essentially independent of time. For mixed conduction it increases with time but tends to stabilize at some finite value, which is the electronic contribution [23]. Therefore, ρ_{dc} for all the compositions was measured at constant temperature ($T = 363$ K) as a function of time using platinum foil electrodes [24], which block ionic conduction. The typical results for $x = 0.2$, 0.3, 0.4, and 0.5 are shown in figure 5(b). It was observed that ρ_{dc} increases

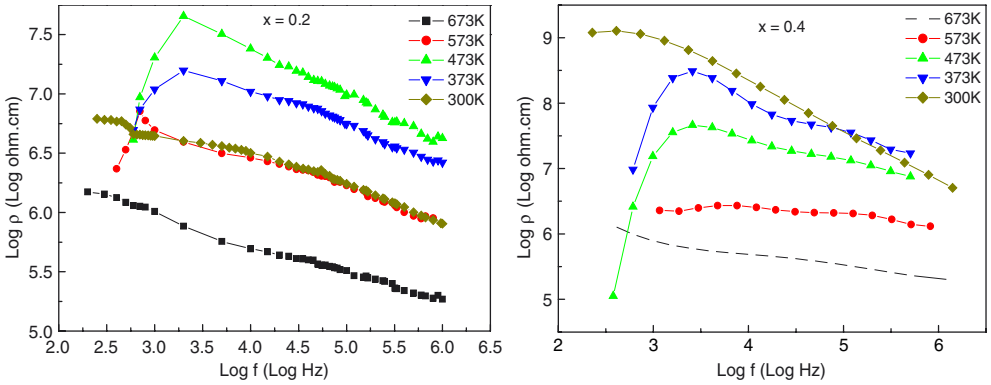

Figure 4. Pellet electrical resistivity versus applied signal frequency ($\log f$) for two representative compositions, $x = 0.2$ and 0.4.

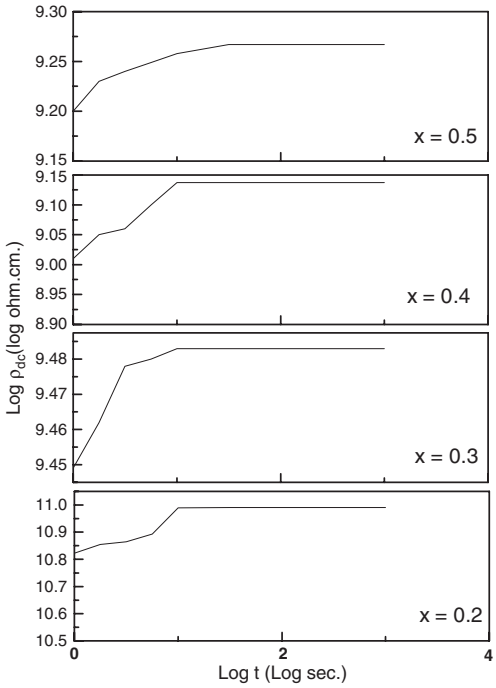

Figure 5. Electrical resistivity as a function of time at 363 K for $x = 0.2$, 0.3, 0.4 and 0.5 compositions.

with time but becomes almost constant after 30 s. The ratio of instantaneous, $\rho_{dc}(0)$, to steady state, $\rho_{dc}(\infty)$, electrical resistivity varies from 0.92 to 0.95 for different ferrites at different temperatures. This indicates that the synthesized ferrite samples are essentially electronic conductors and ionic conduction remains less than 9% at all temperatures.

3.2.1. Thermal variation of dc resistivity measurement. The dc electrical resistivity of pellets of each ferrite made at pressure (P) $\approx 2 \times 10^7$ kg m^{-2} and sintered at 1100 °C for 12 h was measured as a function of temperature (300–700 K). The resistivity values for a particular

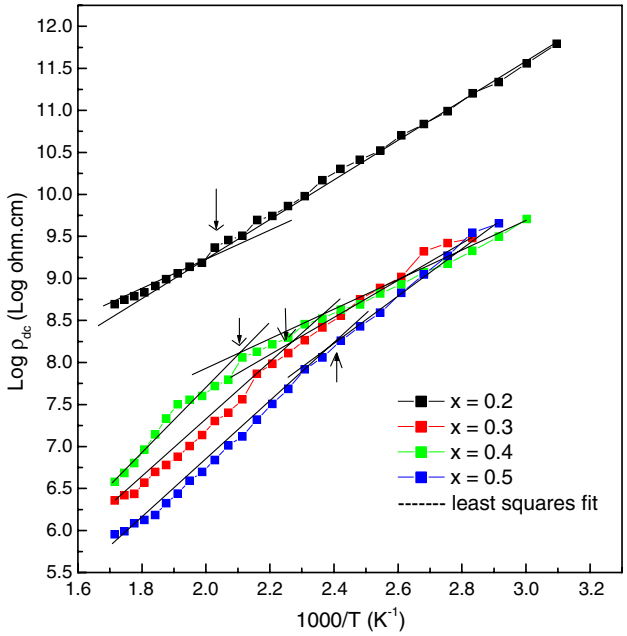

Figure 6. Electrical resistivity (ρ_{dc}) versus temperature for $x = 0.2, 0.3, 0.4$, and 0.5 compositions.

ferrite do not differ much from sample to sample. Furthermore, for each pellet no significant difference was observed for heating and cooling cycles. The ρ_{dc} values for a series of ferrites lie between 10^7 and 10^9 Ω cm near room temperature (table 4); obviously they are good insulators at room temperature. The ρ_{dc} variations with temperature for compositions $x = 0.2$–0.5 are presented in figure 6 as plots of $\log\rho_{dc}$ against $1000/T$. For all the compositions the curves show two slopes with a single transition, which is close to the Néel temperature of the ferrites. The Néel temperature (T_N) deduced for the compositions with $x = 0.2$, 0.3, 0.4 and 0.5 from $\log\rho_{dc}$ versus $1000/T$ plots are listed in table 4. It is found that the values of T_N are in good agreement with those found experimentally from ac susceptibility measurements [17] and theoretically by applying molecular field theory (table 4).

As shown in figure 6, the plot consists of two straight-line portions; hence there are two activation energies for the two different regions. The reason for the two slopes can be explained as follows. At high temperature, the thermal energy is sufficiently great to create vacancies and the activation energies represent a sum of the energies required for vacancy generation and the motion of electrons into the vacancies. At lower temperature, the thermal energy is only large enough to allow the migration of electrons into vacancies already present in the crystal. A change in the slope may be due to the Néel temperature [25] or to the change in the conductivity mechanism [26]. This anomaly strongly supports the influence of magnetic ordering upon the conduction process.

The temperature dependence of resistivity is given by the Arrhenius equation

$$\rho = \rho_o \exp(E_a/kT)$$

where ρ_o is the pre-exponential factor with the dimensions of Ω cm, k is the Boltzmann constant, E_a is the activation energy and T is the absolute temperature.

The activation energies for conduction are computed from $\log_{10}\rho_{dc}$ versus $1000/T$ plots and are presented in table 4. The activation energy increases on changing from the ferrimagnetic

Table 3. Interionic distances between cation–anion (M_e–O) and cation–cation (M_e–M_e).

Content	M_e–O (Å)				M_e–M_e (Å)				
(x)	p	q	r	s	b	c	d	e	f
0.2	1.9501	2.0284	3.8839	3.6795	2.9426	3.4505	3.6040	5.4059	5.0968
0.3	1.9478	2.0352	3.8971	3.6834	2.9442	3.4524	3.6059	5.4089	5.0995
0.4	1.9459	2.0402	3.9065	3.6860	2.9451	3.4534	3.6070	5.4105	5.1011
0.5	1.9431	2.0489	3.9232	3.6910	2.9472	3.4559	3.6096	5.4144	5.1047

(E_f) to paramagnetic (E_p) region. According to the theory of magnetic semiconductors, one expects such a reduction in the activation energy as the system undergoes the transition from the paramagnetic to the ferrimagnetic state. This is due to the fact that the ferrimagnetic state is an ordered state while the paramagnetic state is disordered; thus charge carriers require more energy for the conduction. The high value of the activation energy in the paramagnetic state as compared to the ferrimagnetic state is due to the volume expansion of the samples during the magnetic transition [27, 28]. The activation energies in the ferrimagnetic region are much higher than the ionization energies ($E_i = 0.1$ eV) of donors or acceptors and hence the possibility of band type conduction is ruled out. These values are also higher than the transition energy of Fe^{2+} and Fe^{3+} ($E_e = 0.2$ eV), which indicates that the polaron type conduction mechanism is favoured.

In ferrites, cations are surrounded by close-packed oxygen anions, and as a first approximation can be treated as isolated from each other. There will be little direct overlap of the anion charge clouds or orbitals. Alternatively, the electrons associated with particular ions will largely remain isolated and, hence, a localized electron model is more appropriate in the case of ferrites rather than the collective electron (band) model. In ferrites, the charge carriers are not completely free but are strongly localized in the d-shell; this localization may be due to the electron–phonon interaction (or formation of polarons). A small polaron defect is created when an electronic carrier becomes trapped at a given site as a consequence of the displacement of adjacent atoms or ions. The entire defect (carrier plus distortion) then migrates by an activated hopping mechanism. The small polaron model also explains the low value of mobility, temperature independent Seebeck coefficient and thermally activated hopping. An essential condition for the formation of a small polaron is that the polaron radius (r_p) should be less than the interionic distances. An attempt has been made to calculate the polaron radius for all the compositions studied by the relation [29]

$$r_p = \frac{1}{2}\left[\frac{\pi}{6N}\right]^{1/3}$$

where N = number of sites per unit volume = $96/a^3$.

In spinel ferrites 64 A-sites (tetrahedral) and 32 B-sites (octahedral) are available per unit volume. The calculated values of r_p for $x = 0.2$, 0.3, 0.4 and 0.5 are summarized in table 4. It is seen that these values are smaller than the interionic distances (table 3), and hence are appropriate for small polaron conduction. Furthermore, in the large polaron model, the resistivity is by band conduction at all temperatures and the ac resistivity increases with frequency. The small polarons conduct in a band-like manner up to a certain temperature, the resistivity showing a decrease with frequency. At higher temperatures, the conduction is by thermally activated hopping [30–32]. It is clear from figure 4 that ρ_{ac} decreases with increasing frequency, giving indirect support for small polaron conduction involving a band-like mechanism. Another important indirect confirmation of small polaron formation is that the

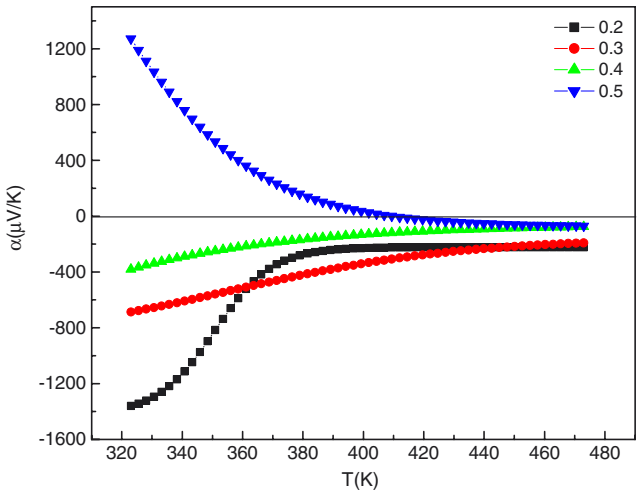

Figure 7. Thermal variation of Seebeck coefficient for $x = 0.2$, 0.3, 0.4 and 0.5 compositions.

Table 4. The Néel temperature (T_N), jump length (L), dc resistivity (ρ_{dc}), activation energy (E) and polaron radius (r_p) for the Zn–Co–Fe–Al–O system.

Zn content (x)	T_N (K) (Theo.)	T_N (K) $\pm$ 5 K susceptibility [17]	T_N (K) $\pm$ 5 K resistivity	L (Å)	ρ_{dc} (Ω cm) (413 K)	E_f	E_p (eV)	ΔE	r_p (Å)
0.2	506.0	510.0	500.0	2.9426	2.01×10^{10}	0.401	0.208	0.193	0.7324
0.3	472.0	470.0	470.0	2.9442	4.16×10^{8}	0.293	0.503	0.210	0.7328
0.4	438.5	435.0	440.0	2.9451	3.92×10^{8}	0.298	0.492	0.194	0.7330
0.5	409.0	410.0	415.0	2.9472	1.82×10^{8}	0.323	0.509	0.186	0.7335

Seebeck coefficient (α) is almost independent of temperature for $T > 340$ K (figure 7). It is interesting to note that for both compositions, in the low frequency region ($f < 4$ kHz) the ac resistivity increases with frequency. For $x = 0.2$ this enhancement in resistivity is observed for $T \leqslant 573$ K, while for $x = 0.4$ this limit is $T \leqslant 473$ K. This feature is indicative of the formation of large polarons in the system, revealed in the low temperature and frequency regime.

It is important to note that small changes in ΔE with x are observed for the present system (table 5). According to Ahmed *et al* [33], the effect of x on ΔE is greater if the substituted cations occupy B-sites. Devale *et al* [34] suggest that almost no change in ΔE is observed when the substitution is made on A-sites without disturbing the B-sites. The small change in ΔE with x for the present system suggests that Zn^{2+} ions occupy A-sites with small disturbance in B-sites, as confirmed by the cation distribution formula (table 2).

3.2.2. Thermoelectric power measurement. The Hall effect and thermoelectric properties are widely used in the interpretation of the conduction mechanism in semiconductors; however, in the case of low mobility semiconductors such as ferrites, it is sometimes difficult to measure the Hall effect: in such cases the thermoelectric measurement technique is the only alternative. Moreover, the measurement of thermo-emf is simple and its sign gives vital information about the type of charge carriers (electrons or holes) responsible for conduction in semiconductors.

Table 5. Ferrous to ferric ion concentration, ferrous ion concentration and electric field strength for $x = 0.2$–0.5 compositions.

Zn content (x)	$[Fe_B^{2+}/Fe_B^{3+}]$ $\times 10^{-2}$ (413 K)	$[Fe_B^{2+}]$ (wt%)	E (V cm^{-1})
0.2	6.56	1.10	No switching
0.3	3.09	0.49	1172.41 (at 673 K)
0.4	23.35	3.52	2000.00 (at 673 K)
0.5	65.09	9.09	545.45 (at 773 K)

As mentioned earlier, the thermoelectric power (α) is negative for samples with $x = 0.2$–0.4, indicating that the majority charge carriers are electrons. Thus the conduction mechanism for the n-type semiconductor is due to the electron transfer between Fe^{2+} and Fe^{3+} ions at the octahedral sites. For the sample with $x = 0.5$, α is positive up to $T = 393$ K, indicating that the majority charge carriers are holes and the conduction mechanism is due to the hole transfer from Fe^{4+} centres to neighbouring Fe^{3+} ions at the B-sites [35]. The thermoelectric voltage (ΔE) developed across each pellet of the ferrite material does not significantly depend upon the heating and cooling cycle and reproducible values (within $\pm 10\%$) are obtained in successive observations. The Seebeck coefficient, α ($\alpha = \Delta E/\Delta T$, where ΔT is the temperature difference across the sample), at different temperatures (300–550 K) for the samples studied is shown in figure 7. The common features of the system studied are that (i) α is negative, and (ii) α decreases with increasing temperature for all the compositions.

The first observation suggests that majority charge carriers are electrons or n-type conduction is dominant. The decreasing negative values for all the compositions may be due to the recombination of some holes and electrons on increasing temperature, since both electrons and holes are responsible for conduction in these samples. As a result accumulation of charges on the respective hot and cold surface reduces. This reduces the thermoelectric voltage across the sample and in turn the Seebeck coefficient.

Bashikirav and Liberman [36] have classified ferrites as degenerate semiconductors if the thermo-emf is independent of temperature and as non-degenerate semiconductors if the thermo-emf depends on temperature. In the present study the samples are non-degenerate semiconductors at lower temperature (<380 K) while they become degenerate for higher temperatures studied (figure 7).

In the region where conduction is due to one kind of charge carrier (electrons or holes; not both) the relations between the Seebeck coefficient (α) and Fermi energy (E_F) will be given by [37, 38]

$$E_F = e\alpha T - AkT$$

where A is a term connected with the kinetic energy of the charge carriers, and e, k and T are the charge of the carrier, Boltzmann constant (8.6×10^{-5} eV) and absolute temperature, respectively. The calculated values of E_F as a function of temperature for two values of A ($A = 0$ and 2) are shown in figure 8. The extrapolated values of E_F to $T = 0$ K yield the values of E_F (0). For the $x = 0.5$ composition, we have taken into consideration the temperature range ($T > 393$ K) for which conduction is only due to electrons.

An alternative and interesting but less familiar way to understand the conduction mechanism, and particularly the charge carriers responsible, is to study the capacitance versus various bias voltage relationship for that composition [39–41]. Figure 9 shows the plot of $1/C^2$ versus bias voltage for all the compositions at 300 and 473 K. The slope of the curve for all compositions at 300 K is negative for the present bias voltage range, indicating that conduction

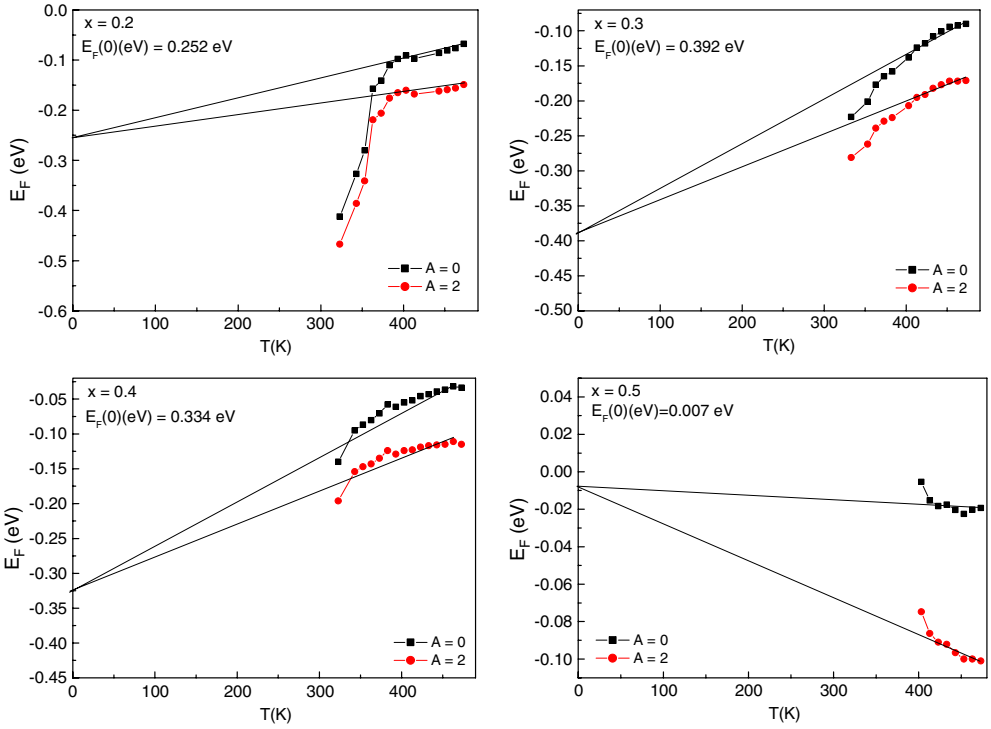

Figure 8. Temperature dependence of Fermi energy (E_f) for $x = 0.2, 0.3, 0.4$ and 0.5 compositions.

is only due to the electrons, and hole conduction is negligible. These results are consistent with thermoelectric power measurements. We find that the curve is almost flat at 473 K for all the samples. These observations suggest that at low temperature or at low bias voltage electrons alone take part in the conduction while both electrons and holes take part in the conduction at high bias voltages or at high temperatures. The holes can contribute to the conductivity only at high bias voltage or at high temperature because of their low mobility.

3.2.3. Temperature variation of charge carrier concentration and mobility. For the hopping mechanism, the Seebeck coefficient, α, is independent of temperature and its magnitude primarily depends upon the density of the charge carriers. It is expressed in the form of the Heikes formula [42]:

$$n_c = \frac{N}{V_s}\left[\frac{1}{1+\exp\left(\frac{\alpha e}{k}\right)}\right]$$

where V_s is the volume of the sample under study.

The values of charge carrier concentration per unit volume have been calculated for all the compositions at each temperature by using the values of the Seebeck coefficient. N is the density of states: in the case of low mobility semiconductors like ferrites having exceedingly narrow bands or localized levels, the value of N can be taken as 10^{28} m^{-3} [43, 44]. The plots $\ln(n_c)$ versus T for various mixed ferrites are shown in figure 10. It can be seen from the figures that the carrier concentration behaves inversely as compared to the variation of Seebeck coefficient with temperature. Here, it should be noted that, for the determination of n_c, only

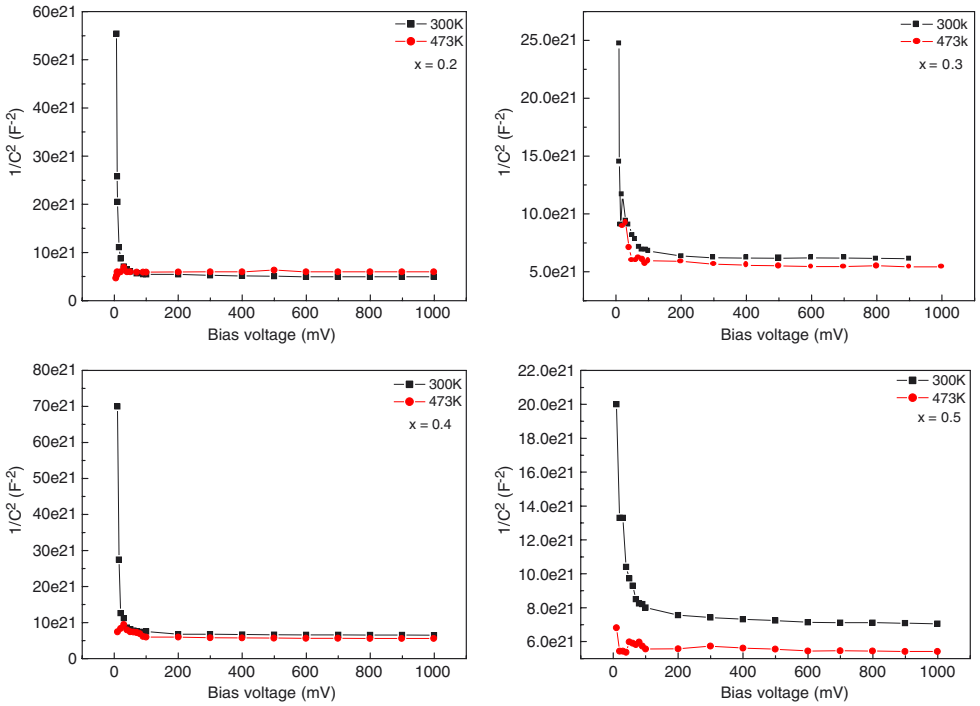

Figure 9. $1/C^2$ versus bias voltage plot for $x = 0.2$, 0.3, 0.4 and 0.5 compositions at 300 and 473 K.

the magnitude of α should be taken into consideration, because positive and negative signs just indicate whether the charge carriers are holes or electrons, and have nothing to do with its value. It is seen that for all the compositions the charge carrier concentration per unit volume increases with increasing temperature. The observed variation of n_c with temperature can be explained on the basis that, on increasing the temperature, the generation of electrons may be expected, supported by the experimental decrease in resistivity.

The mobility (μ_D) of the charge carriers was calculated from the experimental values of the electrical resistivity (ρ_{dc}) and carrier concentration (n_c), using the formula $\mu_D = 1/\rho_{dc} n_c e$, where e is the electric charge of the electron.

The semi-logarithmic representation of the above equation ($\ln \mu_D$ versus $1000/T$) is shown in figure 11 for $Zn_xCo_{1-x}FeAlO_4$ ferrite samples. The figure shows that initially μ_D decreases up to a certain temperature and than increases with further increase in temperature. The observed increase in mobility with temperature is expected and is related to the thermal activation of hopping; on the other hand, the initial decrease in μ_D up to a certain temperature is due to the fact that in ferrites, the charge carriers are not completely free but are strongly localized in the d-shell; this localization may be due to the electron–phonon interaction that hinders the motion of charge carriers. The magnitude of the mobility is found to be in the range 10^{-10}–10^{-12} cm^2 V^{-1} s^{-1} for all compositions. The magnitude is much smaller that suggested for electrons (10^{-4} cm^2 V^{-1} s^{-1}) or holes 10^{-8} cm^2 V^{-1} s^{-1} [45]. This supports the formation of small polarons, in accordance with earlier results.

The thermoelectric power (α) of Zn-substituted cobalt ferrialuminates is directly correlated to the concentration of ferrous and ferric ions in B-sites, as shown in the following

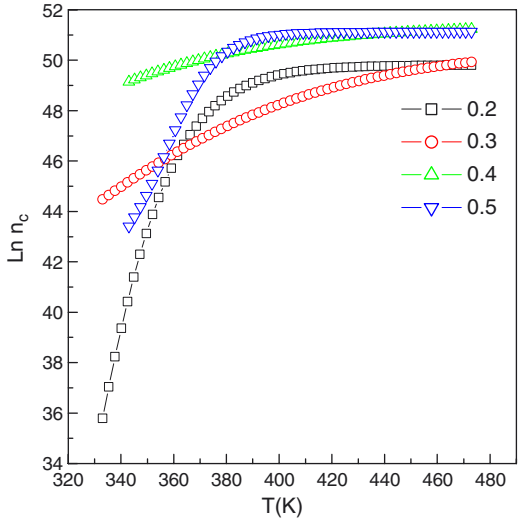

Figure 10. Variation of charge carrier concentrations with temperature for $x = 0.2$, 0.3, 0.4 and 0.5 compositions.

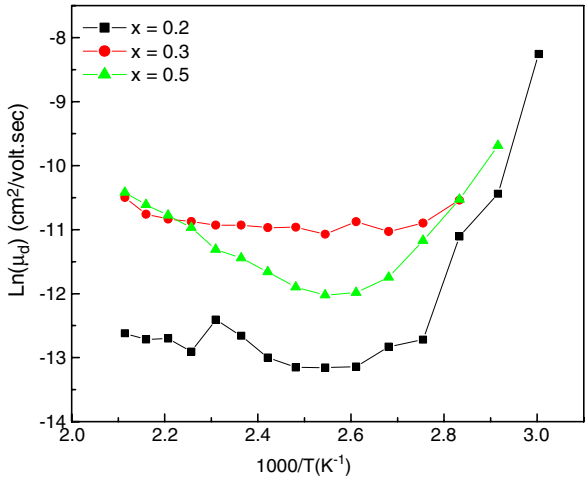

Figure 11. Thermal variation of mobility for $x = 0.2$, 0.3, and 0.5 compositions.

equation [46, 47]:

$$\left[\frac{\mathrm{Fe_B^{3+}}}{\mathrm{Fe_B^{2+}}}\right] = \exp\left(-\frac{\alpha \cdot e}{k}\right). \tag{5}$$

The square bracket denotes the ionic concentration per lattice molecule of $Zn_xCo_{1-x}FeAlO_4$ ($x = 0.2$–0.5), and the subscript B represents the octahedral sublattice of the spinel structure. In equation (5), it was assumed that the small polaron conduction mechanism dominates, as in the present case, and it takes into account only the configurational entropy of electrons, presumably randomly distributed among the octahedral Fe_B^{2+} ions [47]. It is noteworthy to mention that the contribution of Co^{2+} ions to the thermoelectric power is negligible in comparison to that of the Fe ions in ferrite.

The ratio of the ferrous ion (Fe^{2+}) concentration to that of the ferric ion (Fe^{3+}), $[Fe_B^{2+}]/[Fe_B^{3+}]$, was calculated based on equation (5) using Seebeck coefficient values at selected temperatures, and is listed in table 5. The ratio $[Fe_B^{2+}/Fe_B^{3+}]$ increases from 6.56×10^{-2} for $x = 0.2$ to 65.09×10^{-2} for $x = 0.5$ at 413 K. Although we have the ratio $[Fe_B^{2+}/Fe_B^{3+}]$, the estimation of the ferrous ion concentration is not straightforward. In general, the absolute concentration of the ferrous ion is obtained by chemical analysis [48, 49]; in our present study, however, we have estimated the absolute concentration of the ferrous ion by following the procedure suggest by Byeon *et al* [50]. The calculated concentration of Fe_B^{2+} increases from 1.1 wt% for $x = 0.2$ to 9.09 wt% for $x = 0.5$. Here it is evident that the variation in the value of Fe_B^{2+} is around 88%. This suggests that if the variation in resistivity originates from the change in ferrous ion concentration with Zn content (x), it cannot exceed 88%. On the other hand, resistivity data showed a variation close to two orders of magnitude (figure 6). From these results, it can be concluded that the decrease in resistivity values of ferrite samples is mainly due to the increase in ferrous concentration, while the 10% misfit in the resistivity data may be due to the decrease in grain boundary resistivity. The decrease in grain boundary resistivity arises from a small oxygen deficiency due to the evaporation of the Zn ions, as discussed earlier. The electrical conduction in ferrites is known to arise from the small polaron hopping between ferrous and ferric ions present in the octahedral sites of the spinel structure. Based on the model proposed by Klinger *et al* [51] and Tuller *et al* [52], for the electrical conductivity it is not the ferrous ion concentration but the product of Fe^{2+} and Fe^{3+} ion concentrations at B-sites that is of importance. The ferrous ion concentration estimated in this way is found better than the ferrous ion concentration determined by wet-chemical analysis since the former accounts for only the ferrous ions in the octahedral sites.

3.2.4. I–V characteristic measurement. The phenomenon of electrical switching was observed in furnace-cooled samples at high temperature. The plots of current versus electrical field (E), rather than current versus voltage, for these samples are presented in figure 12. This makes it easy to compare the samples of different thickness at a glance.

It is evident from the figure that for the composition with $x = 0.2$, no switching phenomenon is observed in the electric field and temperature range studied. For the compositions with $x = 0.3$ and 0.4 switching was recorded at 673 K, while for $x = 0.5$ it was to be recorded at 773 K. This happened because the switching electric field for $x = 0.5$ went to a much higher value at $= 673$ K. This explains the lower value of the electric field for switching at higher temperature $T = 773$ K (table 5). It suggests that the switching field increased with increasing Zn content (x). Earlier it has been predicated that switching is a structure sensitive phenomenon [53]. It can be seen that, on increasing the Zn content from $x = 0.3$ to 0.5, the required electric field for switching increases. This may be due to the subsequent increase in the size of the unit cell, as is evident from table 1.

From the cation distribution formulae (table 2), it is clear that increasing the Zn content (x), having strong A-site preference, in the system, reduced the Co^{2+} and Fe^{3+} ion concentrations from the B-site; this limits the electron exchange between $Fe^{3+} \leftrightarrow Fe^{2+}$ ions, and as a result, the required electric field for switching increases.

The I–E behaviour of any material at low electric field is linear (ohmic) due to the presence of thermally generated carriers. The observed non-ohmic (nonlinear) I–E characteristics can be explained on the basis of the space charge limited current in inhomogeneous solids which contain grain boundary layers. It is believed that in our case the observed nonlinearities in the I–E characteristics are due to the contact resistance, if any, which is negligible compared to that of basic material.

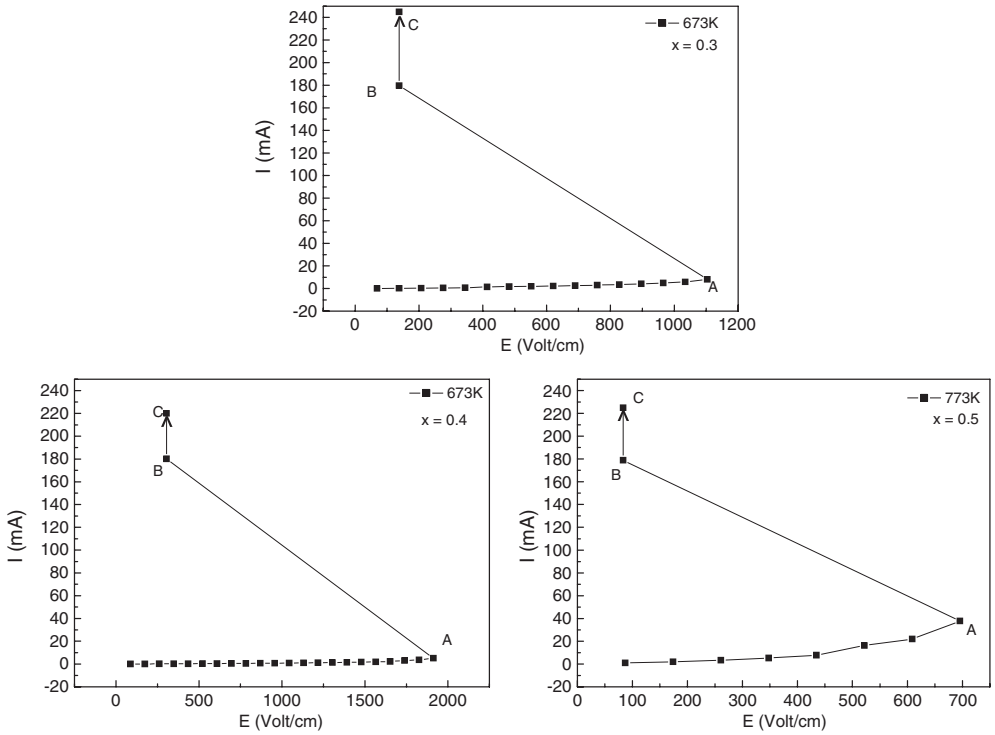

Figure 12. Current (I) versus electric field (E) relationship for $x = 0.3$, 0.4 and 0.5 compositions.

According to the band structure of solids, an insulator is characterized by a full valence band separated from an empty conduction band by a forbidden energy gap of a few electron volts. Evidently, conduction cannot take place in either the field or empty band unless additional carriers are introduced. Carriers may be generated inside the insulator or injected from the metal electrode or from metal insulator contact [54] (bulk limited process). The simplest mechanism is the direct quantum mechanical tunnelling of electrons from one metal electrode to the other. When the injection into the conduction band or tunnelling is not the rate limiting process for conduction in insulators, a space charge build up of the carriers in the valence band or at trapping centres (Fe^{4+}) may occur, which will oppose the applied voltage and impede the charge carrier hopping. At low applied field, with a thermally generated free carrier density, Ohm's law is obeyed, and when the injected carrier density is greater than the free carrier density the current becomes space charge limited. In insulators, as in semiconductors, a significant numbers of lattice defects capable of accepting one or more charge carriers may be present. These charge trapping centres must obviously modify the equilibrium concentration of the carriers and thus space charge limited currents flow in an imperfect insulator.

From figure 12 we can see the nature of the switching phenomenon in the ferrite compositions. The deviation from Ohm's law becomes more prominent with increase of voltage across the sample when the electric field is just over the value indicated by A in figure. For the first cycle, the breakdown suddenly occurs and field falls to the value indicated by B, denoted as the first breakdown field; after this, the current increases monotonically, from B to C. Since the switching current is ∼179 mA for different compositions at different temperature and the properties of the samples were found not be altered even when the cycle was repeated after two

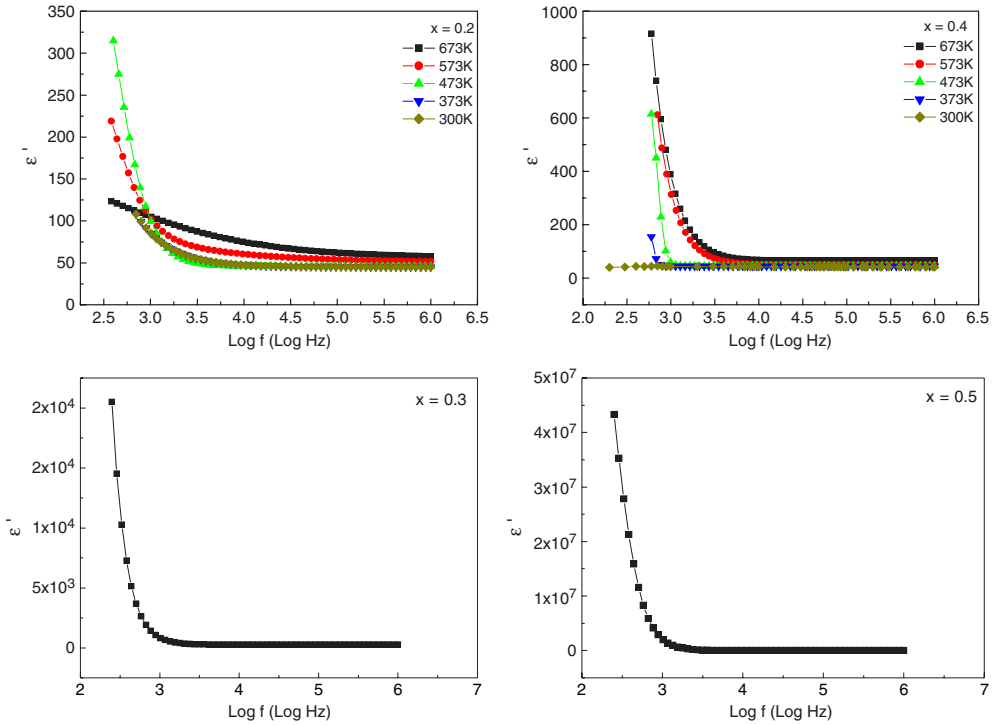

Figure 13. Dielectric constant versus frequency curves at selected temperature for $x = 0.2$ and 0.4 compositions. Dielectric constant versus frequency curve at 300 K for $x = 0.3$ and 0.5 compositions.

weeks, explanations in terms of Joule self-heating and specific resistance of the samples do not appear to be tenable.

In the view of the fact that many different systems exhibit this phenomenon, it will be rather difficult to point out any particular property as being a case of electrical switching and it may be different for different systems. In general, systems with Jahn–Teller ions like Cu^{2+} and Mn^{2+} are probable candidates for switching action. The system under investigation is a Jahn–Teller ion free system, thus this phenomenon cannot be attributed to Jahn–Teller ions, as suggested by Yamashiro *et al* [55]. The structural transformation observed by Vaingankar *et al* [53] also cannot be accepted as the general cause of this phenomenon as neither composition exhibited any structural transformation at any temperature; otherwise, it would have been reflected in temperature dependent dc resistivity measurements.

Further, taking into consideration all the possibilities, we feel that the electron exchange taking place between Fe^{2+} and Fe^{3+} ions on octahedral (B) sites, is responsible for the enhancement of conductivity in these ferrites. Finally, the nature of the I–E characteristics exhibit slow switching which can be thought of due to current controlled negative resistance (CCNR) type while fast switching can only be expected with voltage controlled negative resistance (VCNR) type.

3.3. Dielectric properties

The variation of dielectric constant (ε') with frequency in the range 100 Hz–1 MHz at different temperatures for $x = 0.2$ and 0.4 compositions is shown in figure 13. The variation of ε' with

frequency reveals the dispersion due to Mexwell–Wagner [56] type interfacial polarization, which is in agreement with Koops' phenomenological theory. The large values of ε' at lower frequency are due to the predominance of species like Fe^{2+}, Cu^{1+} ions, interfacial dislocation pile ups, oxygen vacancies, grain boundary defects, etc [57, 58]. The value of ε' decreases with increase in frequency, reaching a constant value for all the compositions (figure 13). This is obvious because of the fact that the only species contributing to the polarizability are bound to be lagging behind the applied field at higher frequency. According to Novikova *et al* [59], the polarization in ferrites is through a mechanism similar to the conduction process. The exchange of electrons between ferrous ions (Fe^{2+}) and ferric ions (Fe^{3+}) on the octahedral site may lead to local displacement of electrons in the direction of the applied field and these electrons determine the polarization. The polarization decreases with increasing frequency and then reaches a constant value due to the fact that beyond a certain frequency of external field the electron hopping cannot follow the alternating field.

In the present system the dispersion in ε' with frequency can be attributed to the Maxwell–Wagner type interfacial polarization, i.e. the fact that inhomogeneities give rise to a frequency dependence of the conductivity because charge carriers accumulate at the boundaries of less conducting regions, thereby creating interfacial polarization.

On the other hand, maximum polarization is observed at higher temperature. This normal dielectric behaviour has been observed in many ferrites [60]. The hopping or exchange of the charge carriers in the octahedral sites, which is responsible for electric conduction, is thermally activated by an increase in temperature. As a result, the dielectric polarization increases, causing an increase in ε' with increasing temperature.

Plots of complex dielectric constant ($\varepsilon'' = D\varepsilon'$) versus $\log f$ (frequency in Hz) for $x = 0.2$ and 0.4 compositions at selected temperatures are shown in figure 14. It is seen that for the $x = 0.2$ composition at 473 K, and for $x = 0.4$ at 573 and 673 K the loss peak occurs at different frequency. A careful examination of the spectra suggests the following.

(i) The peak position shifts towards lower frequency on increasing the temperature.
(ii) The peak intensity increases with increasing temperature.
(iii) For $x = 0.2$ and 0.4, the dielectric loss maximum is not observed for $T < 473$ and 573 K respectively. This suggests that on increasing the Zn content (x), the occurrence of the peak takes place at higher temperature.
(iv) On increasing the Zn concentration for Co^{2+} in the system, the peak position shifts towards higher frequency.
(v) The non-occurrence of the loss peak for $x = 0.2$ at 673 K may be due to the fact that it occurs below the frequency range studied.

According to the Debye relaxation theory, the loss peak occurs when the applied field is in phase with the dielectric and the condition $\omega\tau = 1$ is satisfied, where $\omega = 2\pi f$, f being the frequency of the applied electric field. The observed decrease in ε'' values with frequency after a particular frequency (f_{max}) and increase in ε'' values with increasing temperature, which are the common feature of all the compositions, can be explained on similar lines of argument as for ε'.

The shifting of f_{max} towards the high frequency side can be explained as follows. The relaxation time τ is related to the jumping probability per unit time p by the equation $\tau = 1/2p$ or $f_{max} = p/\pi$. This shows that f_{max}, proportional to the hopping probability per unit time, is increasing continuously. This is probably due to the fact that the concentration of Fe^{2+} ions on the octahedral sites, which are responsible for polarization in those ferrites, increases with increasing Zn content, as confirmed by our thermoelectric power measurements. On the other hand, shifting of the loss peak towards the low frequency side on increasing the temperature

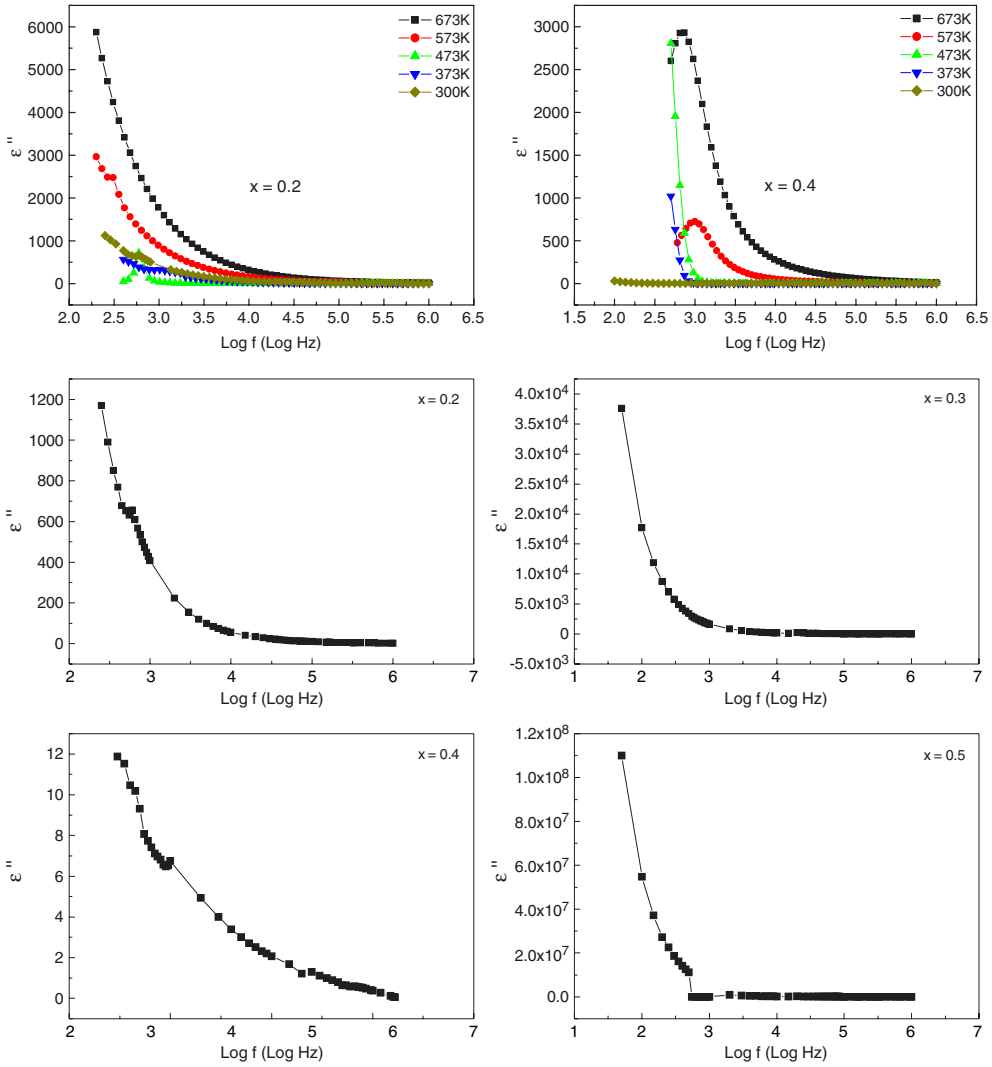

Figure 14. Complex dielectric constant versus frequency curves at selected temperatures. Complex dielectric constant versus frequency curve at 300 K for $x = 0.2$–0.5 compositions.

is due to thermally activated hopping enhancement; as a result resonance takes place at low frequency. The observed broadening of the relaxation peak on increasing Zn substitution suggests strengthening of the dipole–dipole interaction, which makes the dipole orientation difficult. This explains the delayed relaxation of the dipoles giving rise to a broad hump around their dielectric anomaly.

3.4. Electric modulus

3.4.1. Complex impedance plots. The complex impedance Z can be represented as $Z^* = Z' - \mathrm{i}Z'' = |Z|\cos\theta - \mathrm{i}|Z|\sin\theta$, where Z' and Z'' are the real and imaginary parts of complex impedance, and $|Z|$ and θ are the modulus and complex angle of the complex impedance, respectively. The complex impedance formalism helps in determining interparticle interactions

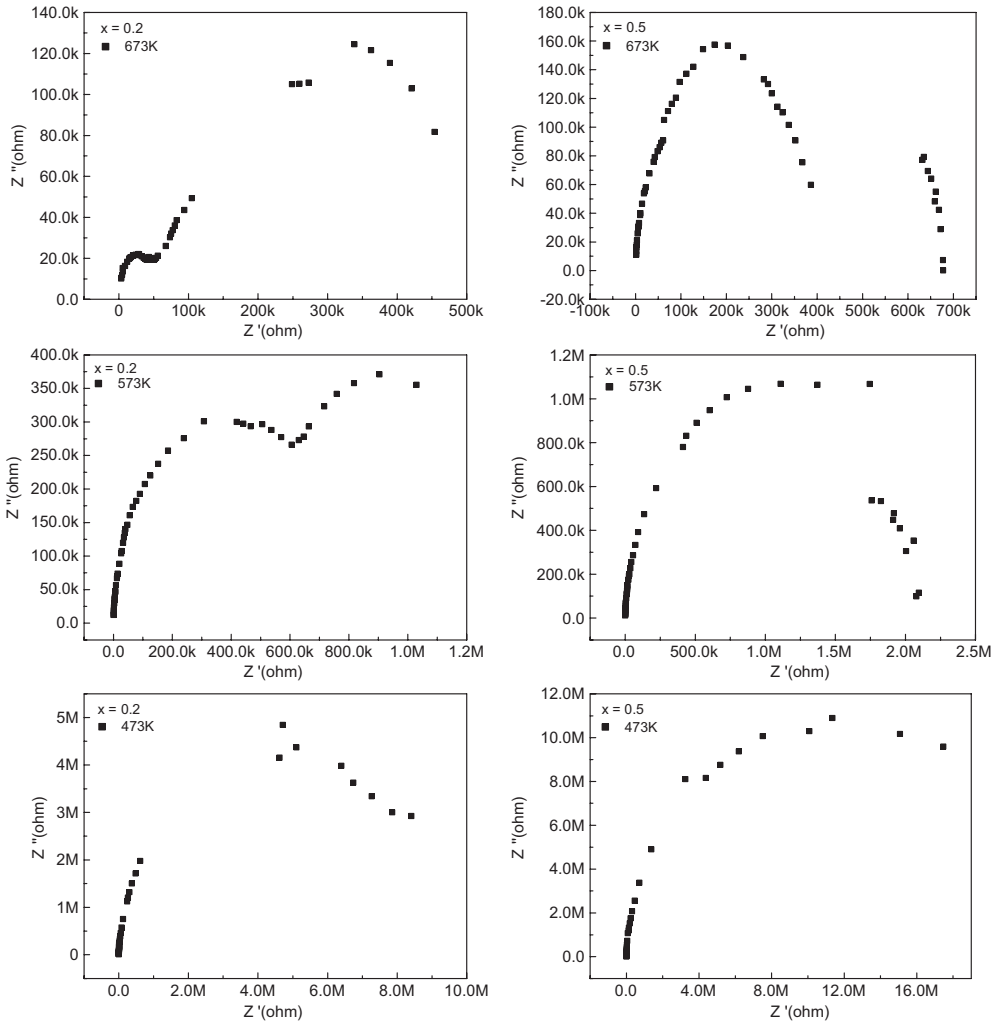

Figure 15. Nyquist diagram (Cole–Cole plots) for $x = 0.2$ and 0.5 at different temperatures.

like grains, grain boundary effects, etc. To study the contribution due to different effects, Cole–Cole analyses have been done at different temperatures. These also provide information about the nature of dielectric relaxation.

Figure 15 shows the imaginary part of the impedance (Z'') versus the real part of the impedance (Z') plotted over a wide frequency range at several temperatures, for all the compositions. It is seen that at 300 K, the impedance data do not take the shape of a semicircle, but rather present a straight line with large slope, suggesting the insulating behaviour of ferrite compositions at room temperature, supported by the resistivity measurements. It is observed that with increase in temperature the slope of the lines decreases and they curve towards the real (Z') axis, and at temperatures above 425 K for $x = 0.2$ and 525 K for $x = 0.4$, a semicircle could be traced, indicating a decrease in resistivity of the sample. At higher temperature ($T > 573$ K) two semicircles could be obtained with different values of resistance for grains and grain boundaries. Thus, the grain and grain boundary contributions could be

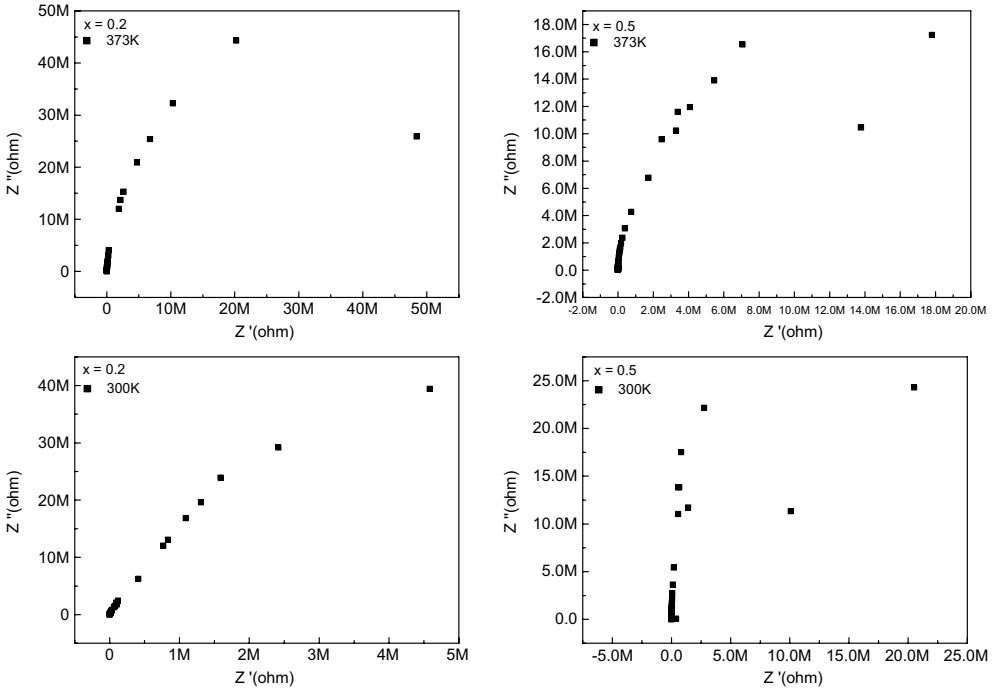

Figure 15. (Continued.)

separated at these temperatures. The intercept of the semicircle with the real axis (Z') at low frequency represents the sum of the resistance of grains and grain boundaries, while the intercept at high frequency represents the resistance of the grains only. A third semicircle could also be seen at 675 K for the $x = 0.2$ composition, which could be due to an electrode effect [61, 62]. The materials used for making holders or electrodes, such as copper or stainless steel, have a small effect on the impedance spectra. This effect may appear as the shift of the spectrum along the Z' axis (x-axis) and the minor segment at the low frequency end. These experimental findings (more than one semicircle contributes to the plot (figure 15)) suggest that the monitoring conduction mechanism is of complex nature. More then one mechanism contributes to the measured dielectric response. Therefore when an attempt has been made to scale of the data (looking for a master curve) and the fitting of the data with the macroscopic theoretical models [61], the results were found to be unsatisfactory in the present case.

The complex impedance (Z^*) measured by an LCR meter can be expressed as the following function of the R_{gb}, R_g, C_{gb}, and C_g of the specimen.

$$Z' = \frac{R_g}{1 + \omega^2 R_g^2 C_g^2} + \frac{R_{gb}}{1 + \omega^2 R_{gb}^2 C_{gb}^2}$$

$$Z'' = \frac{\omega R_g^2 C_g}{1 + \omega^2 R_g^2 C_g^2} + \frac{\omega R_{gb}^2 C_{gb}}{1 + \omega^2 R_{gb}^2 C_{gb}^2}$$

where $\omega = 2\pi f$ and f is the frequency, R_g and C_g are the resistance and capacitance of the grain while R_{gb} and C_{gb} are that of grain boundary. Depending upon the relative rate of decrease of R_g and R_{gb}, and at the same time the relative rate of increase of C_g and C_{gb}, with ω as the variable, the complex impedance curves gradually and successively change from one shape to the other [63], at different temperature.

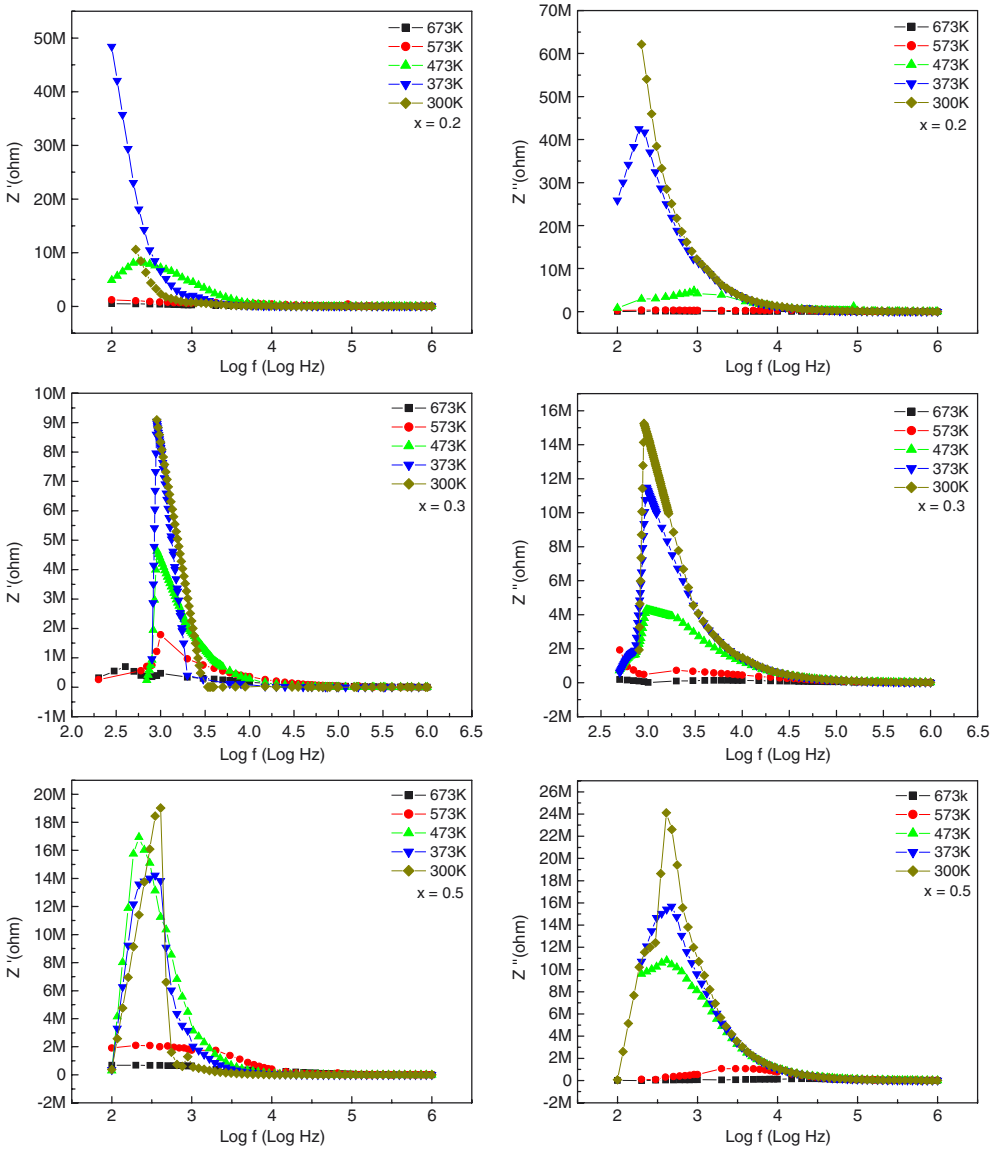

Figure 16. Variation of the imaginary part (Z'') and real part (Z') of the impedance with frequency at different temperatures for $x = 0.2$, 0.3 and 0.5 compositions.

The frequency dependent variation of the real and imaginary part of the impedance (Z'') at different temperatures is shown in figure 16. The observations based on Z'' versus log f spectra for all the compositions can be summarized as: (i) for $x = 0.2$ and 0.3 curves at 300 and 373 K, and for $x = 0.4$ curves at 300, 373 and 473 K are superimposed; (ii) on increasing the temperature further, the peak intensity decreases and the peak position shifts towards high frequency; (iii) the Z'' values for all temperatures merge above 30 kHz.

The curves show that Z'' exhibits the maximum value for given temperature of measurement at a particular frequency ($Z''_{\max}$) and then decreases continuously with further increase in frequency and temperature. This also indicates the single relaxation process in the

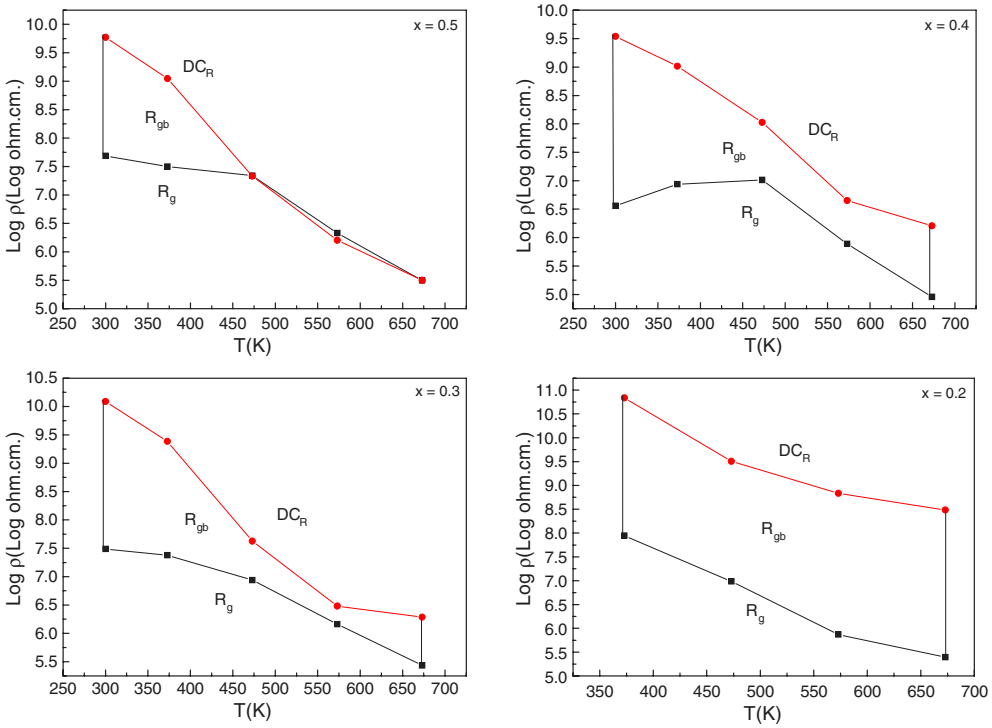

Figure 17. Variation of grain and grain boundary resistance with temperature.

system. The relaxation time (τ) was calculated from the frequency at which $Z''_{\max}$ is observed. The frequency of the maximum shifts to higher values with increasing temperature, indicating the increasing loss in the sample.

According to Von Hipple *et al* [64], in Z'' versus frequency plots, the peak heights are proportional to the grain resistance (R_g), based on the equation

$$Z'' = R_g \left[\frac{\omega\tau}{(1+\omega^2\tau^2)} \right].$$

The relaxation time (τ_m) at peak frequency (ω_m) is defined as $\omega_m \tau_m = 1$.

The value of grain resistance (R_g) calculated from the Z'' versus f plots and dc resistance measured at different temperatures is plotted in figure 17. In the absence of grain boundary resistance (R_{gb}), the bulk resistance from dc measurements (DC_R) and that from impedance plots should match ($DC_R \sim R_g$). The plot shows a difference in the values even at high temperature (except for the $x = 0.5$ composition), indicating the contribution of grain boundary resistance, which is not evident in the complex plane plot which seems to be prominent at still lower frequency range. This result is consistent with the conclusion drawn from the $\rho_{ac}(f, t)$ variation (figure 4).

The variation of the real part of impedance (Z') with frequency at different temperatures is shown in figure 16. Similar to that of Z'', the magnitude of Z' also decreases with an increase in temperature and frequency (beyond the peak frequency), and all the curves coincide for the frequency above 10 kHz. This may be due to the release of space charges. The observed presence of a single peak suggest single relaxation process and indicate an increase in ac conductivity with temperature and frequency.

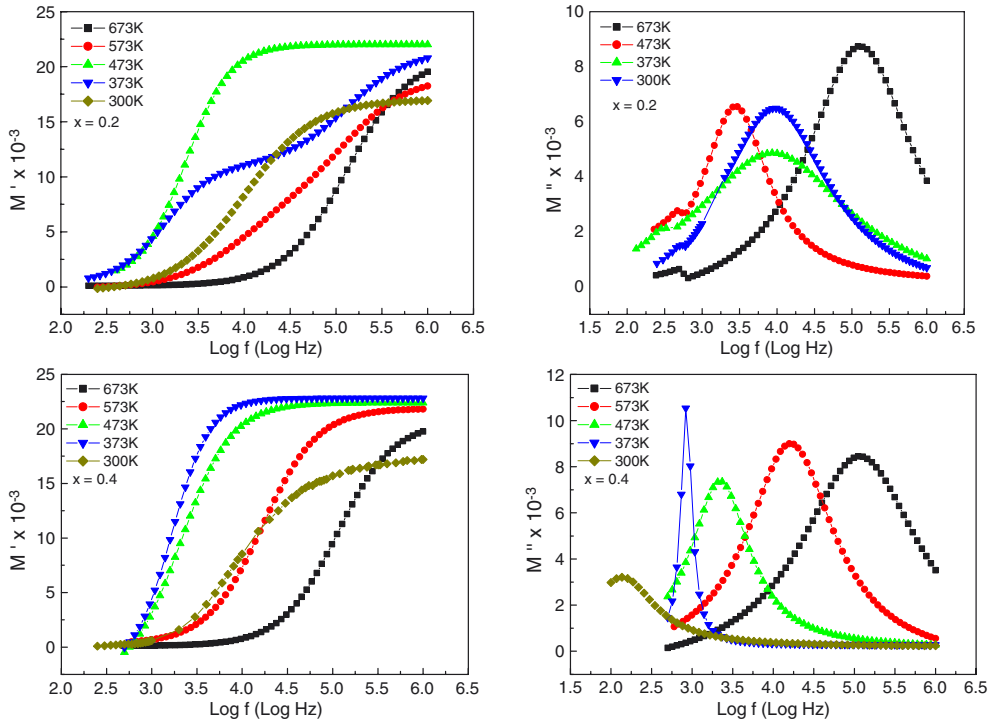

Figure 18. The frequency dependence of the real (M') and imaginary (M'') parts of the dielectric modulus at different temperatures.

3.4.2. Dielectric modulus. The effect of conductivity can be highly suppressed when the data are presented in the modulus representation. Williams *et al* [65] were the first to discuss the reciprocal of complex permittivity as an electrical analogue to the mechanical shear modulus. The dielectric modulus (M^*) corresponds to the relaxation of the electric field in the material when the electric displacement remains constant. Therefore, the modulus represents the real dielectric relaxation process [6]. The complex modulus $M^*(\omega)$ was introduced to describe the dielectric response of non-conducting materials. The usefulness of the modulus representation in the analysis of relaxation phenomenon was demonstrated both for vitreous ionic conductors and polycrystalline ceramics [66].

The starting point for further consideration is the definition of the dielectric modulus:

$$M^*(\omega) = \frac{1}{\varepsilon^*(\omega)} = M'(\omega) + \mathrm{i}M''(\omega).$$

The real (M') and imaginary (M'') parts of the complex electrical modulus were obtained from $\varepsilon'(\omega)$ and $\varepsilon''(\omega)$ values using the relation

$$M'(\omega) = \frac{\varepsilon'(\omega)}{\varepsilon'(\omega)^2 + \varepsilon''(\omega)^2} \qquad \text{and} \qquad M''(\omega) = \frac{\varepsilon''(\omega)}{\varepsilon'(\omega)^2 + \varepsilon''(\omega)^2}.$$

Based on these equations, we have changed the form of presentation of the dielectric data from $\varepsilon'(\omega)$ and $\varepsilon''(\omega)$ to $M'(\omega)$ and $M''(\omega)$. The obtained modulus spectra $M'(\omega)$ and $M''(\omega)$ are depicted in figure 18. Data presented in this way exhibit a pronounced relaxation hump for $M''(\omega)$ that moves towards higher frequencies on heating of the sample for $x = 0.3$–0.5

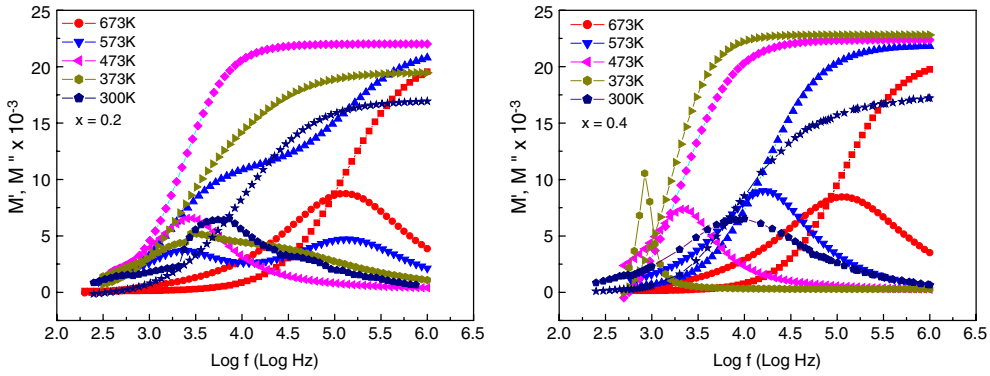

Figure 19. Real (M') and imaginary (M'') parts of the dielectric modulus versus frequency for $x = 0.2$ and 0.4 compositions.

compositions. For $x = 0.2$ the $M''(f)$ peak shifts to lower frequencies with increasing temperature ($T \leqslant 473$ K), whereas for $T > 473$ K it seems to move to higher frequencies with increasing temperature. This behaviour is also observable in figure 4 ($\log \rho$ versus $\log f$ curves) where we observe an increase of ρ_{ac} with increase of temperature up to 473 K. Further increase of temperature results in a decrease of ρ_{ac}. This suggests that the relaxation rate for this process decreases with increasing temperature. The inverse of frequency of the maximum peak position can be taken as a convenient measure of the characteristic relaxation time, i.e. $\tau = 1/2\pi f_c$. The relaxation time thus calculated is found to decrease from 48 μs at 300 K to 1.21 μs at 673 K for the $x = 0.2$ composition, while for $x = 0.4$ it decreases from 1.18 ms to 1.452 μs for the temperature range 300–673 K. Furthermore, it is seen that the relaxation time increases with increasing Zn content in the system at a particular temperature. The magnitude of the peak decreases with increasing temperature as one approaches the Néel temperature, which is a direct indication of increases in the dielectric constant, and thereafter the magnitude goes up with further increase in temperature.

Any change in the stiffness of the material under study is reflected in the spectra of the real part M' of the modulus. The region of frequency where this change occurs is shown by a loss peak in the imaginary part (M'') of the modulus. The full width at half maximum (FWHM) of a suitably normalized $M''(\omega) \rightarrow \omega$ curve gives an idea about the stretched exponent parameter (β) [67]. The value of β helps to decide whether the relaxation present in the material is Debye or non-Debye type. The value of β is equal to unity for an ideal dielectric for which the dipole–dipole interaction is negligible, but the β value is always less than unity for a system in which the dipole–dipole interaction is significant. In our case for all four compositions at different temperatures the β value turned out to be less than unity ($\approx$0.7), showing the presence of the non-Debye nature of the dielectric relaxation. This also suggests a negligible change in average grain size with composition and temperature.

It is important to note that in figure 19 the most prominent relaxation process occurring in the dielectric spectrum is much broader than the simple Debye relaxation. The observed broad relaxation process can be explained on the basis of the fact that (i) it arises from two overlapping peaks, and (ii) it could be a single peak originating from a broad distribution of relaxation time due to a variety of energy barriers resulting from local defects.

We have observed an anomaly (small hump) in the low frequency range (100–600 Hz) for the $x = 0.2$ composition (figure 18) ascribed to the dc conductivity originated process. According to Jonscher [68] and Coelho [69], it is believed that this relaxation process originates

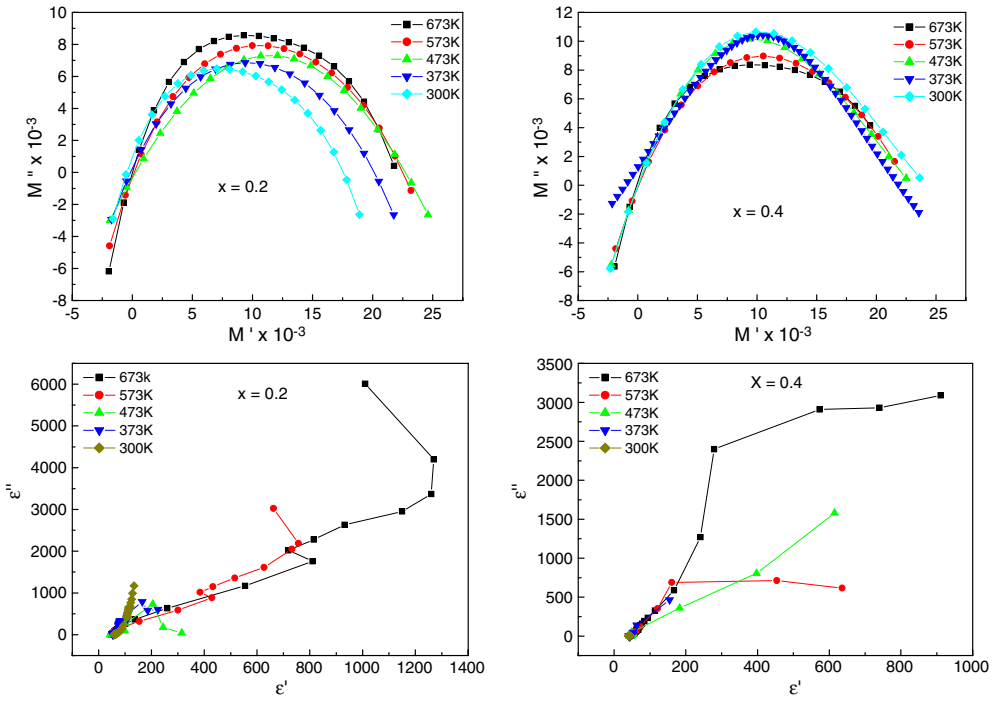

Figure 20. (a) M^* and (b) ε^*, Cole–Cole plots for $x = 0.2$ and 0.4 compositions.

from the dc electric conductivity of a non-homogeneous sample. On the basis of assumption that the relaxation process at low frequency has a simple Debye behaviour, one can determine its characteristic relaxation time ($\tau_{\rm dc}$) [66]. In general, the value of $\tau_{\rm dc}$ is defined by the frequency of the maximum dc peak position f_c. However, we propose the use of the frequency of crossing, $f_{\rm cross}$, of $M'(\omega)$ and $M''(\omega)$ curves, since it is located close to f_c:

$$\tau_{\rm dc} = \frac{1}{2\pi f_{\rm c}} \approx \frac{1}{2\pi f_{\rm cross}}.$$

Thus, an approximate but effective way of estimating $\tau_{\rm dc}$ has been obtained. The logarithm of dc conductivity relaxation times ($\tau_{\rm dc}$) versus reciprocal temperature ($1/T$) dependence has approximately linear characteristics. Thus, the Arrhenius law can be used to described these data satisfactorily: ($\tau_{\rm dc} = \tau_{o,dc} \exp[-E_{\rm dc}/kT]$), with the activation energy equal to $E_{\rm dc} \approx 0.396$ eV and $\tau_{o,dc} = 9$ ns.

The M^* and ε^* Cole–Cole plots for $x = 0.2$ and 0.4 compositions at different temperatures are shown in figures 20(a) and (b). For $M''(f) \rightarrow M'(f)$, the parabolic fitting relation, $M^* = a + bf + cf^2$, f being a applied signal frequency, is satisfactorily valid. The parameters are found to be $a = -0.008\,89$, $b = 1.682\,37$, $c = -0.077\,31$. It is found that the Cole–Cole diagram for $M'(f)$ versus $M'(f)$ is the preferred representation as compared to the $\varepsilon''(f)$ versus $\varepsilon'(f)$ presentation for experimental data of the system under study. The M^* representation shows the semicircle master relation as well as the existence of well defined peaks in $M''(f)$ curves which are satisfactory criteria for an experimentalist for choosing M^* representation.

4. Conclusions

The electrical and dielectric properties of the spinel ferrite system $Zn_xCo_{1-x}FeAlO_4$ have been studied. Summing up the results obtained and conclusions drawn, it is suggested that:

(i) Synthesized ferrite samples are electronic conductors, determined by thermoelectric power and supported by C–V characteristic measurements, large value of activation energy, small value of mobility and frequency dependent conductivity at different temperatures revealing conduction due to the polaron hopping mechanism.

(ii) The switching phenomenon observed for $x = 0.3$–0.5 compositions is current controlled negative resistance (CCNR) type.

(iii) The analysis of electric and dielectric data through complex-plane impedance (Z^*) and dielectric modulus (M^*) provide more insights into the behaviour of the materials, and information regarding the relaxation time, grain and grain boundary contribution to the resistance, and Debye/non-Debye nature of dielectric relaxation. It is found that relaxation time is of the order of microseconds which is the general behaviour of ferrite systems. The magnitude of the stretched exponent parameter ($\sim$0.7) and the depressed semicircles having their centres below the real axis (Z') indicates departure from the Debye behaviour. It is also found that the grain boundary contribution to the resistance is considerable in the frequency and temperature range studied.

(iv) It is found that for experimental data of the system, M^* presentation is the preferred representation as compared to ε^* presentation.

Acknowledgments

One of the authors (KBM) is thankful to AICTE, New Delhi for providing financial assistance under the career award for young teachers scheme and IUAC, New Delhi, IUC-DAE, Indore for financial assistance in the form of research project schemes.

References

[1] Saafan S A, Seoud A S and Shatter R E El 2005 *Physica* B **365** 27
[2] Sidebottom D L, Green P F and Brow R K 1997 *Phys. Rev.* B **56** 170
[3] Neagu R M and Neagu E 2000 *J. Appl. Phys.* **88** 6669
[4] Macedo P B, Moynihan C T and Bose R 1972 *Phys. Chem. Glasses* **31** 171
[5] Whinfrey C G, Eckart D W and Tauber A 1960 *J. Am. Chem. Soc.* **82** 2695
[6] Buerger M J 1960 *J. Crystal Structure Analysis* (New York: Wiley)
[7] Ohnishi H and Teranishi T 1961 *J. Phys. Soc. Japan* **16** 36
[8] Miller A 1959 *J. Appl. Phys.* **30** 245
[9] Trivedi B S and Kulkarni R G 1993 *Asian J. Phys.* **5** 146
[10] Standly K J 1972 *Oxide Magnetic Material* (Oxford: Clarendon)
[11] Globus A, Pascard H and Cagan V 1977 *J. Phys. Suppl.* **438** 439
[12] Sickafus K E and Wills J M 1999 *J. Am. Cream. Soc.* **82** 3279
[13] Goodenough J B 1959 *J. Phys. Chem. Solids* **6** 287
[14] Kanamori J 1959 *J. Phys. Chem. Solids* 10 67
[15] Gilleo M A 1960 *J. Phys. Chem. Solids* **13** 33
Gilleo M A and Geller S 1958 *Phys. Rev.* **110** 73
[16] Baldha G J, Upadhyay R V and Kulkarni R G 1988 *J. Mater. Sci.* **23** 3357
[17] Bhesania R V 2006 *M.Phil. Dissertation* Saurashtra University Rajkot, India
[18] Roberts G G 1974 *Transfer and Storage of Energies by Molecules* vol 4 (New York: Wiley)
[19] Rassel H W 1935 *J. Am. Ceram. Soc.* **18** 1
[20] Gillot B and Jemmali F 1983 *Phys. Status Solidi* a **76** 601

[21] Smit J and Wijn H P 1959 *Ferrites* (The Netherlands: Philips, Tech. Library Clever–Hume Press Ltd)
[22] Heyne L 1977 *Electrochemistry of Mixed Ion Electronic Conductors in Solid Electrolyte* ed S Geller (New York: Springer) p 169
[23] Lal H B, Verma B K and Yadav V R 1982 *J. Mater. Sci.* **17** 3317
[24] Yadav V R and Lal H B 1979 *Cand. J. Phys.* **57** 1204
[25] Komar A P 1954 *Bull. Acad. Sci. USSR. Ser. Phys.* **18** 122
[26] Krishna Murthy K R 1975 *PhD Thesis* IIT, Madras, India
[27] Goodenough J B 1973 *Mater. Res. Bull.* **8** 423
[28] Zemansky M W 1968 *Heat and Thermodynamics* (New York: McGraw-Hill) p 460
[29] Bosman A J and Van Dall H J 1970 *Adv. Phys.* **19** 1
[30] Seitz F, Turnball D and Ehrenreich H 1968 *J. Appl. Solid State Phys.* vol 21 (New York: Academic) p 193
[31] Austin I G and Mott N F 1969 *Adv. Phys.* **18** 41
[32] Mott N F and Davis E A 1971 *Phonons and Polarons in Electronics Processing in Non-crystalline Materials* (Oxford: Clarendon)
[33] Ahmed M A, Nimr M K El, Tawfik A and Hasab A M El 1991 *Phys. Status Solidi* a **123** 501
[34] Devale A B 1980 *PhD Thesis* IISc Nagpur Uni., India
[35] Van Uitert L G 1955 *J. Chem. Phys.* **23** 1883
[36] Bashikirav S S, Liberman A B and Parfenov V V 1979 *Inorg. Mater.* **15** 404
[37] Bosman A J and Crevecoeur C 1966 *Phys. Rev.* **144** 763
[38] Bosman A J and Crevecoeur C 1966 *Phys. Rev.* **144** 763
[39] Na J G, Kim M C, Lee T D and Park S J 1993 *IEEE Trans. Magn.* **29** 3520
[40] Ponpandian N and Narayansamy A 2002 *J. Appl. Phys.* **92** 2770
[41] Ponpandian N and Narayansamy A 2002 *J. Phys.: Condens. Matter* **14** 3221
[42] Heikes R R 1961 *Thermoelectricity* ed R R Heikes and R W Ure (New York: Wiley–Interscience) p 45
[43] Samokhvalov A A and Rustamov A G 1953 *Sov. Phys.—Solid State* **6** 749
[44] Morin F J 1953 *Phys. Rev.* **93** 1195
[45] Ahemed M A, Tawfik A, Nimr M K El and El-Haseb A A 1991 *J. Mater. Sci.* **10** 549
[46] Yoo H-I and Tuller Harry L 1988 *J. Phys. Chem. Solids* **49** 761
[47] Austin I G and Mott N F 1969 *Adv. Phys.* **18** 41
[48] Hoekstra B *et al* 1978 *J. Appl. Phys.* **49** 4902
[49] Ravinder D 1999 *J. Alloys Compounds* **291** 208
[50] Byeon S C, Hong K S, Park J G and Kang W N 1997 *J. Appl. Phys.* **81** 7835
[51] Klinger M I and Samokhvalov A A 1977 *Phys. Status Solidi* b **79** 9
[52] Tuller H L and Nowick A S 1977 *J. Phys. Chem. Solids* **38** 859
[53] Vaingankar A S, Patil S A, Todkar M M, Khot A Y and Devale V B 1980 *Proc. Symp. Nuclear Phys. and Solid State Phys. (New Delhi, India)* vol 23c, p 250
[54] Chopra K L 1969 *Thin Film Phenomena* (New York: McGraw-Hill Book Company)
[55] Yamashiro T 1973 *Japan. J. Appl. Phys.* **12** 148
[56] Koops C G 1951 *Phys. Rev.* **83** 121
[57] Maxwell J C 1973 *Electricity and Magnetism* vol 1 (New York: Oxford University Press) p 828
[58] Wagner K W 1973 *Am. Phys.* **40** 817
[59] Rabinikin L T and Novikova Z I 1960 *Ferrites, Acad. Naok, USSR, Minsk* 146
[60] Hiti M A 1996 *J. Magn. Magn. Mater.* **164** 187 and references therein
[61] Abdullah M H and Yusuff A N 1997 *J. Mater. Sci.* **32** 5817
[62] Prasad N V, Prasad G, Bhimasankaram T, Suryanarayana S V and Kumar G S 2001 *Bull. Mater. Sci.* **24** 487
[63] Wang J, Wu F-Q, Song G, Wu N and Wang J-P 2005 *Ferroelectrics* **323** 71
[64] Von Hipple R 1954 *Dielectric and Waves* (New York: Wiley)
[65] McCrum N G, Read B E and Williams G 1967 *An Elastic and Dielectric Effects in Polymeric Solids* (New York: Wiley)
[66] Molak A, Palunch M, Pawlus S, Klimontko J, Ujama Z and Gruszka I 2005 *J. Phys. D: Appl. Phys.* **38** 1450
[67] Moynihan C T, Boesch L P and Laberge N L 1973 *Phys. Chem. Glasses* **14** 122
[68] Jonscher A K 1996 *Universal Relaxation Law* (London: Chelsea, Dielectric press)
[69] Coelho R 1979 *Physics of Dielectrics* (Amsterdam: Elsevier) chapter 8